



Article title: A simple and quick sensitivity analysis method for methane isotopologues detection with GOSAT-TANSO-FTS

Authors: Edward Malina[1], Jan-Peter Muller[2], David Walton[3]

Affiliations: Imaging Group, Mullard Space Science Laboratory, Department of Space and Climate Physics, University College London, Holmbury St. Mary, Dorking, Surrey, RH5 6NT, UK.[1]

Orcid ids: 0000-0002-1055-4598[1]

Contact e-mail: edward.malina.13@ucl.ac.uk

License information: This is an open access article distributed under the terms of the Creative Commons Attribution License (CC BY) 4.0 <https://creativecommons.org/licenses/by/4.0/>, which permits unrestricted use, distribution and reproduction in any medium, provided the original author and source are credited.

Preprint statement: This article is a preprint and has not been peer-reviewed, under consideration and submitted to UCL Open: Environment Preprint for open peer review.

DOI: 10.14324/111.444/000019.v1

Preprint first posted online: 18 August 2019

Keywords: Methane, Radiative transfer, GOSAT, Isotopologue, SWIR, Education, Outreach, Climate

A simple and quick sensitivity analysis method for methane isotopologues detection with GOSAT-TANSO-FTS

Edward Malina^{1*}, Jan-Peter Muller¹, David Walton¹

¹Imaging Group, Mullard Space Science Laboratory, Department of Space and Climate Physics, University College London, Holmbury St. Mary, Dorking, Surrey, RH5 6NT, UK.

* Currently at ESA/ESTEC, Noordwijk, The Netherlands.

Keywords: Methane; Radiative transfer; GOSAT; Isotopologue; SWIR; Education; Outreach

1. Abstract

Measurements of methane isotopologues can differentiate between different source types, be they biogenic (e.g. marsh lands) or abiogenic (e.g. industry). Global measurements of these isotopologues would greatly benefit the current disconnect between “top-down” (knowledge from Chemistry Transport Models and satellite measurements) and “bottom-up” (in situ measurement inventories) methane measurements. However, current measurements of these isotopologues are limited to a small number of in situ studies and airborne studies. In this paper we investigate the potential for detecting the second most common isotopologue of methane ($^{13}\text{CH}_4$) from space using the Japanese Greenhouse Gases Observation Satellite (GOSAT) applying a quick and simple residual radiance analysis technique. The method allows for a rapid analysis of spectral regions, and can be used to teach University students or advanced school students about radiative transfer analysis. Using this method we find limited sensitivity to $^{13}\text{CH}_4$, with detections limited to total column methane enhancements of $>6\%$, assuming a desert surface albedo of >0.3 .

2. Statement of Robustness

The potential impact of methane and other greenhouse gases (GHGs) on the global environment is recognised at the highest levels of government, shown in the recent signing of the COP21 in Paris. Atmospheric methane is composed of differing isotopic concentrations, with $^{12}\text{CH}_4$ and $^{13}\text{CH}_4$ representing $\sim 99\%$ of total methane concentration. Previous studies have shown that the ratio of these two main ‘isotopologues’ can indicate if the measurement is from a biological or non-biological source. Therefore the exploitation of this known ratio using new measurement techniques on current GHG measuring satellites is timely as well as necessary; potentially allowing for source apportionment on a global scale. This paper demonstrates a unique assessment towards determining the feasibility retrieving the main methane isotopologues concentrations in the Earth’s atmosphere, using the nadir-sounding instrument Greenhouse Gases Observing Satellite – Thermal and near Infrared Sensor for Carbon Observations – Fourier Transform Spectrometer (GOSAT-TANSO-FTS). The methods used in this paper are designed so that advanced school students or

1 early University students can easily apply the methods, which is important in the
2 context of science outreach and citizen engagement.

3 **3. Introduction**

4
5 The impact of methane on the environment and its potential for global warming is well
6 documented (IPCC, 2014). Wuebbles and Hayhoe (2002) state that the increasing levels
7 of methane in the atmosphere significantly affects levels of ozone, water vapour (in the
8 stratosphere), hydroxyl radicals, and numerous other compounds in the atmosphere
9 which result from the oxidation of methane (Bréas et al., 2001). All of these occurrences
10 lead to detrimental effects on the chemistry of the atmosphere (for example the
11 formation of tropospheric ozone, and the depletion of atmospheric methane sinks), as
12 well as the absorption of Infra-red (IR) radiation causing atmospheric heating (Bréas et
13 al., 2001). The total global methane budget is not currently well understood, exemplified
14 by multiple contrasting theories for the stall of the global methane concentration
15 between 2000 and 2006 after a century of increase, and then a subsequent rise from
16 2014 (Nisbet et al., 2016). Aydin et al. (2011) suggest that the drop in global methane
17 output is due to a reduction in the fossil fuel sources of methane, through observations
18 of global concentrations of ethane, which can be used as a global indicator of
19 anthropogenic methane. However in a completely contrasting view, Kai et al. (2011)
20 assert that the reduction in global methane output is in fact due to a reduction in
21 microbial methane from the northern hemisphere; while Mcnorton et al. (2016); Rigby
22 et al. (2012); Turner et al. (2017) suggest that fluctuating hydroxyl radical
23 concentrations is a potential cause of global methane variations. It is therefore
24 important to understand how and where methane is released, and to develop more
25 sophisticated methods of methane detection that will allow for greater understanding of
26 the processes behind methane generation, and how they will affect the global
27 environment.

28
29 Methane gas may be formed through multiple natural and anthropogenic processes,
30 including microorganism decomposition of cellulose in sediments under reducing
31 conditions, the breakdown of gas hydrates including clathrates, and thawing permafrost
32 in arctic and subarctic conditions. Other important processes include, geological
33 processes in the Earth's crust reaching the surface through features such as mud
34 volcanoes or soil exhalation, catagenesis, metamorphism of coal and dispersed organic
35 matter, as well as during petroleum maturation. Anthropogenic sources such as industry
36 bi-products (e.g. leaks from gas plants) and agriculture (e.g. livestock or rice paddy
37 fields) must also be considered as highly significant (Archer et al., 2009; Bréas et al.,
38 2001). Industrial bi-products imply that fossil fuels can be detected by the type of
39 methane gas given off by their formation and exploitation (Kort et al., 2014; Rella et al.,
40 2013). Towards this end many satellite missions have been focused on trying to
41 measure fossil fuel sources by their methane emissions, including the Japanese
42 Greenhouse Gases Observation Satellite (Kuze et al., 2009; Turner et al., 2015), which
43 was designed specifically for this purpose.

44
45 Atmospheric methane consists of a number of different isotopologues (molecules that
46 vary according to their isotopic composition), the main four being $^{12}\text{CH}_4$ accounting for
47 roughly 98% of atmospheric methane, $^{13}\text{CH}_4$ making up roughly 1.1% of atmospheric
48 methane and CH_3D , present in very small concentrations (roughly 0.06%), with all the

1 other isotopologues present in tiny amounts. The ability to distinguish spectroscopically
2 between the isotopologues of methane can potentially allow the determination of the
3 nature of the source of methane emissions (either biogenic, thermogenic or abiogenic),
4 by taking the ratio of the concentration of $^{12}\text{CH}_4$ and $^{13}\text{CH}_4$ isotopologues (Etiope and
5 Ciccioli, 2009; Nisbet et al., 2016; Schwietzke et al., 2016). This method has been used
6 effectively for *in situ* terrestrial studies previously and it is this relationship that is the
7 focus of this study. Currently there are limited global measurements of separated
8 methane isotopologues, the majority of measurement sites falling under the National
9 Oceanic and Atmospheric Administration
10 (NOAA) (www.esrl.noaa.gov/gmd/ccgg/trends_ch4/) as well as a small number of other
11 independent organisations (Nisbet et al., 2016). Based on this limited spread of
12 measurement sites, the existence of a satellite instrument that can differentiate between
13 methane isotopologues would expand the global knowledge of methane distributions. It
14 has been achieved in the upper troposphere and lower stratosphere with solar
15 occultation limb viewing instruments (Buzan et al., 2016; Irion et al., 1996), and is hoped
16 to be achieved with dedicated potential future instruments (Weidmann et al., 2017).

17
18 The aim of this paper is to identify spectral regions where the main methane
19 isotopologues ($^{12}\text{CH}_4$ and $^{13}\text{CH}_4$) can be detected with the existing GOSAT Thermal and
20 Near Infrared Sensor for carbon Observation Fourier Transform Spectrometer (GOSAT-
21 TANSO-FTS). Such studies are typically performed using the Information Content (IC)
22 analysis method described in (Rodgers, 2000), examples of which are also reported in
23 (Herbin et al., 2013; Malina et al., 2018; Yoshida et al., 2011). IC analysis is a powerful
24 tool, but has several significant challenges associated with its use. Firstly, on its own the
25 IC analysis cannot be used to estimate atmospheric trace gas concentration since it is an
26 analysis method and not a full retrieval algorithm (such as (Parker et al., 2011; Schepers
27 et al., 2012; Yoshida et al., 2011)). Secondly, there is a substantial step in effort required
28 to convert the IC analysis method into a retrieval tool capable of trace gas estimation (in
29 terms of computation, analysis methods etc). The current algorithms used to produce
30 trace gas concentrations from instruments such as GOSAT-TANSO-FTS or the recently
31 launched Sentinel-5P/Tropospheric Monitoring Instrument (TROPOMI) are the results
32 of multi-year efforts, built on experience with older instruments (e.g. the SCanning
33 Imaging Absorption SpectroMeter for Atmospheric CHartography (SCIAMACHY) or
34 similar). Therefore, new research into satellite trace gas retrieval must rely on one of
35 these well-established algorithms, or embark on an expensive development program.

36
37 In this paper we propose to use a simple residual radiance analysis technique to identify
38 the suitability of GOSAT-TANSO-FTS for detecting $^{13}\text{CH}_4$, and the ratio of $^{13}\text{CH}_4$ and $^{12}\text{CH}_4$
39 known as $\delta^{13}\text{C}$, which is based on the IC analysis method. Although the residual radiance
40 analysis technique is not as sophisticated as the Optimal Estimation Method (OEM) of
41 (Rodgers, 2000), it remains relevant in the context of trace gas detection/retrieval for its
42 ease of use, and quick applicability. Fundamentally, the residual radiance technique is an
43 excellent starting point for getting familiar with the OEM, and could be an important
44 aspect of advanced school students or University students.

45
46 This paper is structured as follows:

- 47 • Section 1 – Introduction.
- 48 • Section 2 – Describes the tools and methods used in this study.
- 49 • Section 3 – Outlines the results.

- Section 4 – Discusses the results and methods from sections 2 and 3.
- Section 5 – Concludes the findings.

4. Experimental Design and Starting Assumptions

4.1. Methane Source Isotopologue Composition

The isotopic composition of atmospheric background methane and methane sources has been studied at some length (Chanton, 2005; Nisbet et al., 2016; Rigby et al., 2012; Röckmann et al., 2011), especially the four key isotopologues $^{12}\text{CH}_4$, $^{13}\text{CH}_4$, $^{12}\text{CH}_3\text{D}$ and $^{13}\text{CH}_3\text{D}$. These papers effectively describe how the ratios of methane isotopologues (often referred to as “ δ ” values) can be used to identify the nature of the source. Normally the metrics $\delta^{13}\text{C}$ and δD are used to define the ratio of isotopologues at the source. The $\delta^{13}\text{C}$ ratio is defined as:

$$\delta^{13}\text{C} = \left(\frac{\left(\frac{^{13}\text{C}}{^{12}\text{C}}\right)_{\text{sample}}}{\left(\frac{^{13}\text{C}}{^{12}\text{C}}\right)_{\text{standard}}} - 1 \right) \times 1000\text{‰} \quad (1)$$

$\delta^{13}\text{C}$ is generated by taking the ratio C13:C12 of the gas sample under investigation, and dividing it by a base ratio (or standard ratio) taken from the established literature known as the Vienna Pee Dee Belemnite, which then determines how far the sample in question deviates from the standard (Craig, 1957). A large negative value indicates that the sample is depleted in C13. Large negative values tend to be associated with biogenic sources of methane, while values closer to 0 are largely from industrial sources.

The methane to deuterium based methane ratio is known as δD is calculated using a similar method to the calculation of $\delta^{13}\text{C}$, this ratio divided by an established base ratio taken from the established literature known as the Vienna Standard Ocean Water. However as stated earlier, deuterium based methane is very rare in the atmosphere, and we decided early on to focus solely on $^{13}\text{CH}_4$ as opposed to CH_3D .

The main reason for the depletion of the heavier isotopologues in biogenic sources is due to the observation that microorganism formation of methane tends to discriminate against ^{13}C due to Kinetic Isotope Effects (KIEs), accounting for the low $\delta^{13}\text{C}$ values. Different forms of microorganisms will have different rates of KIEs, thus changing the $\delta^{13}\text{C}$ values with respect to the exact source, however the precise nature of these KIEs is still poorly understood. In addition, specific plants will vary in their ^{13}C signature due to differing photosynthetic enzymes, partially accounting for the range in $\delta^{13}\text{C}$ values noted in microbial sources (Schweizer et al., 1999; Whiticar, 1999).

4.2. Radiative Transfer Models – SCIATRAN and ORFM

Radiative Transfer Models (RTMs) are a fundamental aspect of this work, and a key aspect of this study is focused on providing trace gas investigation methods for independent research. It is difficult to perform trace gas research without the use of an

1 RTM. Developing an RTM from scratch for this project fulfils neither of the quick or
2 simple goals, and we therefore decided to use an open source RTM.

3
4 In this study we use the SCIATRAN (Rozanov et al., 2014) RTM, developed by the
5 SCIATRAN working group at the Institute of Environmental Physics and the University
6 of Bremen, available from <http://www.iup.uni-bremen.de/sciatran/index.html>.
7 SCIATRAN is an RTM capable of solving the radiative transfer equation using multiple
8 numerical methods. SCIATRAN can simulate satellite solar backscatter radiative transfer
9 in both clear-sky and aerosol loaded conditions. SCIATRAN is versatile and can simulate
10 numerous atmospheric effects such as clouds, fluorescence, advanced bidirectional
11 reflectance distribution functions and others for multiple geometry types. For this study
12 the simulations from SCIATRAN are run at a spectral resolution of 0.01 cm^{-1} and are
13 convolved with a TANSO-FTS type Gaussian Instrument Line Shape Function (ILSF) of
14 0.27 cm^{-1} full width half max (Kuze et al., 2009). All simulations include multiple
15 scattering effects, where all Mie scattering effects assume spherical particles. SCIATRAN
16 has significant pedigree with previous instruments such as SCIAMACHY, and has been
17 previously used in studies relating to GOSAT previously e.g. (Reuter et al., 2012).

18
19 SCIATRAN uses a climatological database derived from a 2D chemistry transport model
20 (CTM) described in (Sinnhuber et al., 2009). All gases, temperatures and pressures are
21 provided in the altitude range 1-95 km for 10° latitudinal bins for all months in a given
22 year. The isotopologue profiles in SCIATRAN are identical to the CH_4 profile included in
23 the simulated atmosphere. The difference in abundance between CH_4 and $^{12/13}\text{CH}_4$ is
24 accounted for in the HITRAN2016 database, which scales the isotopologue line strengths
25 by abundance figures provided by (Bièvre et al., 1984). The advantage of this method is
26 that the complexity of adding an additional trace gas profile to the forward model is
27 reduced, the disadvantage is that this scaling assumes that this abundance ratio is true
28 for the whole globe (which is unlikely to be true).

29
30 Scattering is considered in SCIATRAN, both through Rayleigh scattering and aerosol
31 induced Mie scattering. Rayleigh scattering is not considered in this study as it is minor
32 in the SWIR. For aerosol related scattering SCIATRAN draws upon the LOWTRAN
33 database (Kneizys et al., 1988), which can simulate multiple different aerosol types for
34 different layers of the atmosphere. In this study we assume the standard
35 SCIATRAN/LOWTRAN settings for aerosol loading in SCIATRAN.

36
37 The spectral line database used in this study is HITRAN2016 (Gordon et al., 2017).
38 HITRAN2016 builds upon the HITRAN2012 database, but includes an increase in the
39 number of assigned $^{13}\text{CH}_4$ spectral lines, with Brown et al (Brown et al., 2013) indicating
40 a significant jump in the number of and accuracy of $^{13}\text{CH}_4$ (and $^{12}\text{CH}_4$) spectral lines in
41 comparison to the previous HITRAN iteration (HITRAN 2008; (Rothman et al., 2009)).
42 HITRAN2016 includes data from recent studies such as (Starikova et al., 2016), which
43 contain numerous additional line assignments in the spectral range of GOSAT-TANSO-
44 FTS band 2. However it is not suggested that there are any updates to the $^{13}\text{CH}_4$ line lists
45 in band 4 of TANSO-FTS.

46
47 In addition to SCIATRAN, we also employ the Oxford Reference Forward Model (ORFM;
48 (Dudhia, 2017)), developed at the University of Oxford, and available at
49 <http://eodg.atm.ox.ac.uk/RFM/>. We do not use the ORFM in the residual radiance

1 calculations described in the sections below, but rather to simulate atmospheric
2 transmittance and optical depth. This is because the ORFM allows for quick and easy
3 transmission (and absorption) calculations in all of the wavelengths of interest in this
4 study. ORFM is not used for the residual radiance study since a 'sun' is not included in
5 the radiance calculations, and scattering is not included.

8 **4.3. GOSAT-TANSO-FTS**

9
10 The Japanese Aerospace Exploration Agency (JAXA) launched GOSAT in 2009; GOSAT
11 was the first satellite specifically designed to measure GHG emissions around the globe.
12 The GOSAT project is a joint effort between the Ministry of the Environment (MOE), the
13 National Institute for Environmental Studies (NIES), and JAXA (Kuze et al., 2009; Yokota
14 et al., 2009). GOSAT originally had a 6 year lifespan, but has since been extended. Its
15 replacement was GOSAT-2 was launched in October of 2018, but data is as yet
16 unavailable.

17
18 The key instrument on GOSAT is the TANSO-FTS, which measures the radiance of
19 sunlight reflected from the Earth's surface through the atmosphere in three separate
20 bands: the main band of interest in this study is band 2 which measures radiance in the
21 wavenumber range $5814\text{-}6410\text{ cm}^{-1}$ ($1.56\text{-}1.72\text{ }\mu\text{m}$), with a sampling interval of 0.2 cm^{-1} .
22 GOSAT-TANSO-FTS has a fourth band that measures emissions spectra in the Thermal
23 Infrared (TIR) between $699\text{ - }1799\text{ cm}^{-1}$ ($5.56\text{-}14.3\text{ }\mu\text{m}$) (Kuze et al., 2009; Yokota et al.,
24 2009).

25
26 GOSAT has a history of providing reliable estimates of the global distributions of
27 methane and carbon dioxide (Parker et al., 2015, 2016; Schepers et al., 2012; Yoshida et
28 al., 2013) since its launch. With its high spectral resolution and high SNR, GOSAT was
29 judged to be a good candidate for detecting methane isotopologues, and therefore
30 prompted this investigation. There are other instruments for measuring methane
31 isotopologues from orbit e.g. SCIAMACHY and TROPOMI. SCIAMACHY has a significantly
32 lower spectral resolution (1.5 cm^{-1}) and has been found to have poor single sounding
33 precision. Buchwitz et al (Buchwitz et al., 2017) state that SCIAMACHY registers a
34 maximum single sounding measurement precision of 30 ppbv, which is unlikely to be
35 sufficient for the retrieval of $^{13}\text{CH}_4$, where the total column concentration of $^{13}\text{CH}_4$ is
36 roughly 20 ppbv. The recently launched TROPOMI is a possible candidate for methane
37 isotopologues measurements, TROPOMI contains a push-broom spectrometer and
38 sacrifices spectral resolution (0.45 cm^{-1}) for much increased SNR. TROPOMI is likely
39 to be investigated in the future for methane isotopologue detection.

41 **4.4. Study Structure and Methods**

42
43 The following subsection discusses the structure of the research study. The key aims are
44 to show the following under realistic atmospheric conditions:

- 45 a) The optimal regions in bands 2 and 4 of the GOSAT-TANSO-FTS for $^{13}\text{CH}_4$
46 detection.
- 47 b) Measurable changes in $^{13}\text{CH}_4$ spectral lines over and above the background
48 contaminating gases, and GOSAT-TANSO-FTS instrument noise.

1 c) The effects of background contaminate gases on any measurable changes.
2
3

4 **4.4.1. Spectral Region Identification**

5

6 The first step of this study is to make an initial assessment as to where the least
7 contaminated regions for $^{13}\text{CH}_4$ may be found in the SWIR and TIR. The strongest
8 absorption lines for methane in the SWIR are present within the wavebands at 1.6 μm
9 and 2.3 μm (Brown et al., 2013). However the GOSAT-TANSO-FTS sensitivity to methane
10 is limited to 1.6 μm , in band 2. In the TIR region there is a broadband methane
11 absorption feature at 7.7 μm , which is covered by band 4 of TANSO-FTS. We therefore
12 set-up a simulation scenario with ORFM in order to pick out the maximum absorption
13 points for the $^{13}\text{CH}_4$, outlined in Table 1.
14

15 The atmospheric model used in this assessment provides a high number of vertical
16 levels and gas concentrations at more recent magnitudes (2002) than the standard
17 FASCODE mid-latitude model atmospheres (which were designed in the 1970's), and
18 was originally designed to aid in MIPAS retrievals (Remedios et al., 2007). An example of
19 the atmospheric profiles of three gases from this model is shown in Figure 1.
20

21 GOSAT-TANSO-FTS measures the column average density of methane and carbon
22 dioxide (XCH_4 , XCO_2); therefore, using the pressure profiles captured in the UoL MIPAS
23 profile, the column-averaged densities can be calculated.
24

25 The strongest absorption regions of the methane isotopologues are then investigated in
26 order to gain further insight into the influence of contaminant gases on the
27 isotopologues. The ORFM includes the options to simulate absorption as well as
28 radiance, thus giving some insight into the presence of spectral lines of interest. The
29 conditions required to calculate a typical $^{13}\text{CH}_4$ atmospheric absorption profile are
30 specified in Table 1.
31

32 **4.4.2. Detecting Changes in $^{13}\text{CH}_4$ Signal**

33

34 Background simulated radiance values (containing radiance from the main
35 contaminating gases,) are subtracted from the radiances generated from a scenario with
36 elevated concentrations of methane. If this calculated residual difference is greater than
37 the noise radiance known as the Noise Equivalent Delta Radiance (NEDL) then it
38 suggests that GOSAT-TANSO-FTS could detect this change in methane concentration.
39 This is known as the residual radiance technique, and has been demonstrated by both
40 Roberts et al and Leifer et al (Leifer et al., 2006; Roberts et al., 2010) as an effective
41 technique for assessing whether changes in concentrations of trace gases can be
42 detected. Roberts et al (Roberts et al., 2010) states that spectral residuals are often the
43 first step in full atmospheric inversions. Following the method proposed by (Roberts et
44 al., 2010), the residual radiance technique is used to determine the atmospheric
45 conditions when isotopologue retrieval may be possible. The key question to answer is
46 which combination(s) of methane concentration, water vapour concentration and
47 surface reflectance allow for a residual radiance greater than the instrumental noise.
48 This can be determined from the equation below.

$$F_d = |L_b(A, \lambda_m) - L_e(A, \lambda_m)| - NEDL, \quad (2)$$

where F_d is the detection factor, where any value above 0 suggests that some signal is detectable above the noise limit, and therefore constitutes a detection. L_b is the background radiance at the wavelength of the maximum radiance λ_m given reflectance A , L_e is the atmospheric radiance with elevated methane concentrations (see Table 3) at the wavelength of the maximum radiance λ_m given reflectance A and NEDL.

Typically NEDL can be calculated from knowledge of instrument parameters (dark current etc), however these parameters are often kept secret by instrument manufacturers. According to the GOSAT-TANSO-FTS instrument manufacturers at JAXA the GOSAT-TANSO-FTS L1B product (interferograms (L1A data) are converted into radiance spectra via a Fourier transform, including some data screening routines). They contain two separate elements: real spectra (equivalent to the radiance spectra of interest in trace gas retrieval), and imaginary spectra which are equivalent to noise from FTS theory. The implication of this is that the noise from the spectrum of a particular retrieval can be extracted from the L1B spectra. Therefore, we generate a relationship where the noise profile of GOSAT-TANSO-FTS is estimated given a radiance output from real spectra. The steps for generating this profile are as follows: Extract the real and imaginary spectra from several L1B data GOSAT-TANSO-FTS band 2 products, in order to get variation in radiance output based on the location and surface characteristics of the retrieval. Calculate the Root Mean Square (RMS) of the off-band imaginary spectrum radiance (where off band is the region where the Indium Gallium Arsenide detector is not sensitive to the incident radiation due to an optical band pass filter present in the instrument). This is equivalent to the inherent instrument noise, and the RMS of the on-band (which is where the detector is sensitive to measured radiance) real spectrum for multiple retrievals. This builds up a profile of how instrument noise varies with received radiance at the detector (dominated by shot noise). The square of the RMS imagery spectrum radiance values are then plotted against the RMS of the real spectrum radiance values; this builds up a profile of how the noise is dependent on the spectral radiance, as well as highlighting what the basic instrument noise is. This allows for a mathematical relationship to be generated, meaning that for any given particular retrieval radiance, a specific noise value can be attributed to it. Using a random selection of 400 GOSAT L1b spectra downloaded from the GOSAT Data Archive Service (https://data2.gosat.nies.go.jp/index_en.html), the following relationship was calculated.

$$NEDL = \sqrt{(1.76e^{-8}L + 1.358e^{-11})} \times C, \quad (3)$$

where, L is the received radiance (in $W/cm^2/str/cm^{-1}$) and C is a conversion factor from internal GOSAT units into radiance units. The value of C is available on the GOSAT data archive website in the TANSO-FTS Radiometric Conversion for Band 1-3 document (<https://data2.gosat.nies.go.jp/doc/document.html#Document>). In this study the NEDL is assumed to be a constant value over the whole spectral range, and we assume that the GOSAT spectra are captured under high gain conditions.

Equation 2 is based on using individual measurements, which will most likely suffer significantly from noise levels. However as suggested by (Roberts et al., 2010) the NEDL

1 can be reduced by averaging multiple spectral measurements focusing on the spectral
 2 positions with the most $^{13}\text{CH}_4$ information. In such a case the NEDL reduces with \sqrt{n} ,
 3 where n is the number of spectral sampling points, described by Equation 4 (modified
 4 from (Roberts et al., 2010)), below.

$$5 \quad F_d = \frac{\sum_{\lambda=a}^{\lambda=b} (L_b(A, \lambda_m) - L_e(A, \lambda_m))}{n} - \frac{NEDL}{\sqrt{n}}, \quad (4)$$

6
 7
 8
 9 where F_d is the detection factor over an averaged number of spectral bands, n is the
 10 number of spectral bands for combination, between wavelengths a and b. In the normal
 11 operation of GOSAT there is no oversampling of measurement points, until the satellite
 12 returns to the same orbital path (i.e. only one spectrum is captured per sample point). In
 13 this case the method proposed in Equation 4 cannot be used, since repeat measurements
 14 are captured under different conditions. However, Kuze et al (Kuze et al., 2012) describe
 15 non-standard operational modes, one of which includes 3 repeat measurements of the
 16 same point for “sun glint and limited calibration and validation site observations” (Kuze
 17 et al., 2012). Although not all GOSAT data will be captured in this way, for simulation
 18 purposes, it is justified to investigate the effects of averaging 3 concurrently captured
 19 spectra. Indeed, GOSAT has a ‘targeted observations’ mode, where registered
 20 researchers can request observations of specific sites, implying that a large number of
 21 concurrently captured spectra could be obtained with this method. The exact details of
 22 this mode are not published, and are therefore not modelled in this study. Note that the
 23 method described in Equation (4) assumes that errors between spectral points are
 24 uncorrelated.

25
 26 The sensitivity of any $^{12}\text{CH}_4$ and $^{13}\text{CH}_4$ absorption bands to interfering trace gases and
 27 different reflectance conditions must also be considered; the methane absorption
 28 windows in the SWIR are typically heavily influenced by water vapour, and therefore
 29 any absorption by $^{13}\text{CH}_4$ is likely to be affected. The influence of water vapour on specific
 30 $^{13}\text{CH}_4$ absorption peaks can be determined from the simple ratio factor as described
 31 below (modified from (Roberts et al., 2010)).

$$32 \quad S_f = \frac{\frac{\sum_{\lambda=a}^{\lambda=b} L_{res}(W_s, A)}{n}}{\frac{\sum_{\lambda=a}^{\lambda=b} L_{res}(W_e, A)}{n}}. \quad (5)$$

33
 34
 35
 36 Where S_f is the sensitivity factor, $L_{res}(W_s, A)$ is the residual radiance between background
 37 and elevated methane conditions at standard atmospheric conditions between
 38 wavelengths, a and b, $L_{res}(W_e, A)$ is the residual radiance between background and
 39 elevated methane conditions with elevated water vapour concentrations between the
 40 wavelengths, a and b, and n is the number of spectral measurements considered. Note
 41 that this method applies to any desired target and interfering species.

42
 43 It is important to define appropriate atmospheric scenarios in order to determine
 44 feasible detection factors, with the key factors being methane concentration in the
 45 atmospheric profile and surface reflectance. Numerous total column retrieval methods
 46 are based on the ‘scale’ method, where the total column concentration is scaled rather

1 than individual atmospheric layer concentrations modified. Therefore, a range of total
2 column scale factors on which to calculate residuals are specified, appropriate to real
3 world scenarios. The maximum total column XCH₄ values observed from GOSAT tend to
4 be roughly 1900 ppb (Parker et al., 2016), equating to a column scaling of 10% (w.r.t to
5 the MIPAS profile). Very large methane values (>1900 ppb) have been observed by
6 GOSAT in fire affected regions (Parker et al., 2016), suggesting that although >1900 ppb
7 values are possible, they will be found in unique circumstances.

8
9 The second key factor, reflectance, can be determined using the online database created
10 by UCL and Noveltis under contract to ESA called “A surface reflectance Database for
11 ESA’s earth observation Missions (ADAM)” available at <http://adam.noveltis.com/>
12 (Muller et al., 2013). ADAM predicts that the expected Earth surface reflectance values at
13 1600 nm range from 0.1 for densely vegetated areas, to 0.6 for desert regions (e.g. in the
14 USA or the Sahara).

15
16 Based on this range of values, a series of simulation conditions and scenarios were
17 generated as specified in Table 2.
18

19 **5. Results**

20 21 **5.1. Absorption Assessment**

22 23 **5.1.1. SWIR**

24
25 Using the atmospheric conditions specified in Table 1, ORFM was used to focus on the
26 1600-1700nm region. Figure 2 indicates that it will be challenging to resolve ¹³CH₄
27 absorption lines in this spectral region, suggesting that pinpointing ¹³CH₄ absorption
28 above background gases will be difficult. The strongest/most dense ¹³CH₄ lines appear to
29 be at 1658-1659nm and 1670-1671nm. Focusing on these two spectral regions, the
30 optical depth is explored to determine the effect of background absorbers at these
31 specific wavelengths. Figure 3 makes clear that both of the ¹³CH₄ spectral regions
32 indicated have similar optical depth values to those of all of the remaining gases,
33 implying that the majority of absorption in these spectral regions is due to ¹³CH₄.
34 However, the spectral line in the 1658-1659nm wavelength range clearly shows the
35 least interference from background contaminating gases, therefore suggesting that it is
36 more suited for retrieval. In spite of this, it is obvious that the optical depth of the ¹³CH₄
37 lines in this region is very low, and it will therefore be challenging to detect any changes
38 to ¹³CH₄ in this wavelength range.
39

40 **5.1.2. TIR**

41
42 Focusing on the TIR band of GOSAT, we perform a repeat analysis of 4.1.1. Comparing
43 the strength of ¹³CH₄ absorption in the TANSO-FTS TIR wavelength range shown in
44 Figure 4 against that in the SWIR shows a number of striking differences, primarily in
45 the magnitude of the absorption. With the strongest of the ¹³CH₄ TIR lines having
46 absorption strengths x40 of their SWIR equivalents. Despite this, background

1 interference is still strong, dominated by water vapour continuum absorption. We now
2 focus on the optical depth of two regions, the 7700-7800 nm region due to the strength
3 of $^{13}\text{CH}_4$ absorption in this region, and the 8050-8150 nm range due to the lower
4 background absorbance.
5

6 The optical depth survey shown in Figure 5 demonstrates magnitudes far in excess of
7 the SWIR optical depth in Figure 3 (especially Figure 5(a), where the atmosphere is
8 opaque), but as shown in Figures 4 and 5, the background interference on the $^{13}\text{CH}_4$
9 signal is significant, with only minor impacts from the $^{13}\text{CH}_4$ spectral lines. This leaves us
10 with the unenviable position of small optical depth but low background interference in
11 the SWIR, and high optical depth but high levels of interference in the TIR.
12

13 Figure 5 suggests that $^{12}\text{CH}_4$ and other background gases will dominate the residual
14 radiance method for the TIR. Therefore for this reason, and that measurements in the
15 TIR are often more uncertain than SWIR measurements, exemplified in multiple studies
16 (Holl et al., 2016; Ohyama et al., 2013, 2017), we decided to focus on the SWIR in this
17 study. In addition it has been shown that the SNR on the methane absorption regions in
18 GOSAT are significantly lower than in the SWIR (Holl et al., 2016; Zou et al., 2016),
19 suggesting that the TIR is not ideal for methane retrieval with GOSAT. TIR instruments
20 are heavily based on measuring thermal contrast between atmospheric layers, and
21 because of the lack of such contrast in the lower troposphere, therefore have limited
22 sensitivity near the surface (Clerbaux et al., 2009; Worden et al., 2015). This suggests
23 that measurements in the SWIR are far more likely to capture methane fractionation at
24 the surface than in the TIR. There are cases with global scenes with high thermal
25 contrast, which will allow for sensitivity to the surface for TIR instruments, however we
26 believe that the low SNR of TANSO-FTS band 4 is the more important issue, as opposed
27 to surface sensitivity.
28
29

30 **5.2. $^{13}\text{CH}_4$ Detectability under Standard Conditions**

31

32 Based on the simulation conditions specified in Table 2, consideration is given as to
33 whether or not the individual peaks highlighted in Figure 3 will exceed the NEDL.
34 Figures 6 and 7 show example results for two different surface albedos, for all the
35 proposed methane concentration levels.
36

37 The results in Figures 6 and 7 suggest that detecting changes in concentration of $^{13}\text{CH}_4$
38 using individual peaks is unlikely to succeed, with only the highest methane
39 concentrations at the highest albedo levels giving a positive detection and all other
40 residual radiance calculations falling below the NEDL line. However, if we assume the
41 GOSAT sampling pattern which take three concurrent measurements of the same area
42 (Kuze et al., 2012), by applying Equation 4, and using the mean of $^{13}\text{CH}_4$ residual
43 radiance peaks, the NEDL is reduced by $\sqrt{3}$. These are summarised in Table 3.
44

45 Considering the results outlined in Table 3 it is clear that the feasibility of detecting any
46 change in $^{13}\text{CH}_4$ concentration above the NEDL is going to be difficult. The results
47 indicate that the minimum requirements for measuring $^{13}\text{CH}_4$ concentration with any
48 certainty are a methane source of at least 10% higher concentration than background

1 total column value, with a high surface albedo of 0.3. Although such a combination of
2 conditions is possible, it would likely be limited to wildfire regions such as (Parker et al.,
3 2016). Note that the detection factors between the two regions of interest are very
4 similar.

5
6 We note in section 3.2 that HITRAN2016 includes an intensity adjustment for methane
7 isotopologues that accounts for natural atmospheric abundance. We now investigate if
8 the detection factors indicated in Table 3 change, if we assume the standard $\delta^{13}\text{C}$ value is
9 -70‰ as opposed to 0‰ . To achieve this, we modified the isotopologues intensity in
10 HITRAN2016, by assuming Vienna Pee Dee Belemnite is 0.0010326 as opposed to
11 0.0011031. Then we reran the scenarios shown in Table 2; the results for the albedo =
12 0.3 case are shown in Figure 8.

13
14 Figure 8 is interesting because it shows that the $^{13}\text{CH}_4$ peak at 1658.6 nm is highly
15 sensitive to changes in the assumed $\delta^{13}\text{C}$ value, to the point where changes of the
16 methane column concentration has practically no impact on the residual radiance. While
17 the spectral lines at 1670.4 is not as sensitive to the change in $\delta^{13}\text{C}$ value, and as
18 indicated in Table 4, actually shows an increase in the magnitude of the detection
19 factors.

20
21 The HITRAN2016 database suggests that the $^{13}\text{CH}_4$ spectral lines in the 1670.2-1670.6
22 nm are made up of a number of different transitions, which exhibit a range of lower state
23 energy values. A number of which are of similar magnitude to those for the main
24 methane isotopologue $^{12}\text{CH}_4$. While the lower state energy levels for $^{12}\text{CH}_4$ are
25 significantly larger than those for the $^{13}\text{CH}_4$ lines in the 1658 – 1659 nm range, which
26 explains this difference in reactions to changes in the standard $\delta^{13}\text{C}$ values.

27
28 In addition to the simulations for the $\delta^{13}\text{C}$ values of 0‰ and -70‰ , we also performed
29 an analysis for $\delta^{13}\text{C}$ values of -35‰ . Based on the detection factors for the range of $\delta^{13}\text{C}$
30 value shown in this study, we can plot these variables and determine the conditions
31 where GOSAT can detect differences in $\delta^{13}\text{C}$ values.

32
33 Based on the detection values indicated in Tables 3, and 4, and given similar results from
34 an analysis of $\delta^{13}\text{C}$ values of -35‰ . We can plot a relationship between the detection
35 values and the surface albedo for a given $\delta^{13}\text{C}$ value.

36
37 Figure 9 is interesting since it shows that the 1658 nm band has more sensitivity to
38 changes in surface reflectance, and total column methane concentration than the 1670
39 nm band. But only in the case where $\delta^{13}\text{C}$ is assumed to be equal to zero. For the other
40 $\delta^{13}\text{C}$ cases shown in Figure 9, there are no examples where the detection factor is
41 greater than 0. For the 1670 nm band, although the detection factors are lower in
42 magnitude, the sensitivity to changes in the $\delta^{13}\text{C}$ are minor. These results imply
43 (focusing on the 1670 nm band), that given a significant enhancement in the total
44 methane column, and a high enough surface reflectance, it may be possible to detect
45 changes in the $\delta^{13}\text{C}$ of the measurement. Since the detection factor can be related back to
46 a total methane column value, $\delta^{13}\text{C}$ values could be directly estimated. Assuming some
47 knowledge of $^{12}\text{CH}_4$. Figure 9 suggests that the lowest possible surface albedo of 0.35,
48 requires an enormous methane enhancement of 8% in order to achieve a detection of
49 $^{13}\text{CH}_4$, while the highest surface albedo of 0.6 requires an enhancement of 5 or 6%.

1
2 The required surface conditions to achieve the above values are not common. Using the
3 aforementioned ADAM dataset (<http://adam.noveltis.com/>), we can indicate how much
4 of the Earth's land surface has surface albedo values of at least 0.3. The database
5 suggests that a significant proportion of the Earth has >0.3 surface albedo. Significantly
6 the biomass burning regions indicated in (Parker et al., 2016) have the required surface
7 albedo, thus suggesting that in the scenarios observed in (Parker et al., 2016) it would
8 be possible to detect $^{13}\text{CH}_4$ signals with GOSAT using the methods described in this
9 paper.

12 5.3. $^{13}\text{CH}_4$ Detectability under High Water Vapour Conditions

13
14 Using Equation 5 we can interpret the potential effects of varying water vapour
15 concentration on the spectral averaging factor, given the high water vapour
16 concentration conditions specified in Table 3. Based on the sensitivity factors indicated
17 in Table 5, it is clear that both of the spectral bands we investigate in this paper are
18 affected by the increase in loading of water vapour to some degree. The 1658 nm band is
19 affected to a far less extent than the 1670 nm band (~10%). Most likely because the
20 1658 nm band is narrower than the 1670 nm band. For both bands the scaling of the
21 methane column has a negligible effect, meaning that the high methane scenarios
22 required to detect $^{13}\text{CH}_4$ will not be subject to water vapour errors, any more than high
23 surface albedo scenarios. The loading of the water vapour column by 100% is not an
24 unreasonable scenario when considering the difference between mid-latitude scenes
25 and tropical scenes.

27 6. Discussion

28
29 The range of scenarios where $^{13}\text{CH}_4$ can be detected is very small. We acknowledge that
30 this method is not as sophisticated or as accurate as a full sensitivity analysis using
31 Rodgers optimal estimation method. However we argue that the benefits of the method
32 shown in this study is its simplicity, such that a quick analysis can be performed by a lay
33 person interested in the subject area, or it could be used to teach advanced school
34 students, or early year University students. Indeed scientists interested in quickly
35 determining the sensitivity of a trace gas species could use this method as a quick first
36 step, before committing to further analysis. The most complex part of this study is the
37 RTM, and here we use two well established RTMs to achieve the goals of this study. RTM
38 development is a far more complex task than developing a retrieval algorithm, and
39 independently developing an RTM would no longer make this study simple or quick.
40 There are significantly more open source RTMs available than retrieval algorithms, this
41 variety in RTMs mean that there should be sufficient ranges in solutions and methods
42 that allow for characterisation of any errors in the forward models.

43
44 The detection analysis outlined in section 3.4.2 is based on the total column of methane
45 detection of $\delta^{13}\text{C}$, this method is potentially limiting to a degree since this does not take
46 into account KIEs in the upper troposphere and lower stratosphere due to the
47 destruction of methane. However, since $^{13}\text{CH}_4$ concentration is low, and the KIE factors
48 are less than those at the surface, such factors are unlikely to have a significant impact

1 on the results. In addition atmospheric air currents interfere with the total column and
2 thus will dampen the signal of $\delta^{13}\text{C}$ in the total column, as opposed to in situ
3 measurements. There are currently no studies that investigate this effect, but we can
4 assume that the $\delta^{13}\text{C}$ differences between source types will be even smaller.
5

6 Other error sources include the spectroscopy and the forward model. The HITRAN2016
7 database in combination with the SCIATRAN forward model assumes a Voigt profile for
8 all methane lines in the GOSAT spectral sensitivity ranges. The Voigt profile has been
9 generally assumed for methane spectral regions in the past, however this shape is now
10 acknowledged to be no longer sufficient (Gordon et al., 2017). The current HITRAN2016
11 database does not include the parameters necessary to estimate non-Voigt line shapes
12 for methane; however it is anticipated that future updates will include these. We
13 therefore accept that there will be spectroscopic errors present in this study. Following
14 on from the HITRAN database, the next largest error sources are likely to arise from
15 SCIATRAN, generated from inaccuracies in recreating the absorption or radiance spectra
16 from a given set of atmospheric inputs.
17

18 The metrics F_d and S_f give a useful indication of the feasibility of detecting $^{13}\text{CH}_4$, and can
19 be used to further inform a user about the feasibility of detection over a wider variety of
20 atmospheric and surface conditions than shown in this study. However, caution must be
21 applied since as highlighted in Table 5, the influence of water vapour on the $^{13}\text{CH}_4$ peaks
22 might well lead to false positive values of F_d , and therefore create an incorrect inference
23 of isotopologues detection.
24

25 Although we briefly looked at methane isotopologues absorption in the GOSAT TIR
26 band, we did not investigate this in depth. This is despite the fact that the isotopologues
27 indicated much larger optical depth than their equivalent in the SWIR. However there is
28 significant evidence to suggest that the spectroscopy of methane in the TIR is not nearly
29 as advanced as that in the SWIR (De Lange and Landgraf, 2018), which is important
30 given the short wavebands used in this study. In addition to the high levels of
31 background interference on the $^{13}\text{CH}_4$ spectral lines observed in Figure 5.
32

33 An obvious next or alternative step would be to perform retrievals of the methane
34 isotopologues using the Total Column Carbon Observing Network (TCCON, (Wunch et
35 al., 2011)). TCCON relies on solar occultation measurements as opposed to solar
36 backscatter, and operates at a much higher SNR and spectral resolution than GOSAT. The
37 key disadvantage to TCCON is that it is limited to a small number of sites all over the
38 globe, and cannot be as beneficial to global studies as satellites such as GOSAT. We
39 believe that a study using TCCON data should be a study in its own right, and does not fit
40 in the context of the demonstration of the quick and simple methods we use in this
41 paper.
42
43

44 **7. Conclusions**

45
46 In this paper we investigated the potential to detect the second most common methane
47 isotopologue ($^{13}\text{CH}_4$) using the GOSAT-TANSO-FTS instrument. The ratio of the main
48 methane isotopologues has been shown to be able to differentiate between different

1 methane source types, and could be a useful tool in linking global bottom-up emissions
2 with top-down emissions.

3
4 We use a simple and quick residual radiance method in order to investigate the benefit
5 of such techniques, in the wider context of the more sophisticated methods based on
6 Rodgers' optimal estimation techniques. We argue that the residual radiance technique
7 is useful as a simple and quick method for analysing spectral regions for sensitivity to
8 specific trace gases.

9
10 The results of this study generally suggest that detecting the second most important
11 methane isotopologue is difficult in most circumstances, apart from unique
12 circumstances such as large biomass burning events. Using these techniques we find
13 that detections of $^{13}\text{CH}_4$ with GOSAT can only occur with surface albedos of >0.3 ,
14 assuming at least an 8% enhancement in the methane total column. This total column
15 requirement is reduced with increasing surface albedo. In the context of a world where
16 El Nino events are likely to become more frequent, it is possible that the required
17 conditions for $^{13}\text{CH}_4$ detection using this technique, may become more common.

18
19 We perform the assessment using the general assumption of $\delta^{13}\text{C} = 0$ globally as this is
20 built into the HITRAN databases. However we also investigate the effects of detecting
21 the $^{13}\text{CH}_4$ isotopologue using different values of $\delta^{13}\text{C}$, ranging up to -70‰ . We find that
22 the spectral lines in the 1670 nm waveband are unaffected by the change in $\delta^{13}\text{C}$, while
23 other spectral regions are significantly affected by this change.

24
25 We also assess the suitability of the TIR region for methane isotopologues, and find that
26 although the optical depth of $^{13}\text{CH}_4$ is greater than that in the SWIR region, the
27 dominance of background trace gases, and the unknowns in the spectroscopy of the
28 region make this region less attractive than the SWIR.

29 30 **Acknowledgments**

31 We would also like to acknowledge Anu Dudhia at Oxford University for the ORFM, the
32 SCIATRAN working group at the Institute of Environmental Physics at the University of
33 Bremen for SCIATRAN, HITRAN for HITRAN2016 and JAXA/NIES/MOE for GOSAT-
34 TANSO-FTS L1B data.

35 36 37 **Funding Statement**

38 This research has been funded under a PhD grant (award number 157550) from the
39 National Centre for Earth Observation (NCEO) through the Natural Environment
40 Research Council (NERC) based in the UK.

41 42 43 **Data Accessibility**

44
45 *HITRAN2016 data is available from <https://hitran.org/>. The OFRM is available through
46 the website <http://eodg.atm.ox.ac.uk/RFM/>. SCIATRAN is available through
47 <http://www.iup.uni-bremen.de/sciatran/index.html>. The GOSAT L1B data is available
48 through the GOSAT Data Archive Service https://data2.gosat.nies.go.jp/index_en.html.*

1 The ORFM and SCIATRAN simulations used in this paper are fully reproducible given the
2 input parameters provided in this paper.

4 **Competing Interests**

5 *'There are no competing interests.'*

8 **Authors' Contributions**

9 E.M., J-P. M. and D.W. conceived and designed the experiments; E.M. performed the
10 experiments, analysed the data and wrote the paper; D.W. contributed code for initial
11 HITRAN line survey analysis. JPM contributed the reflectance analysis.

17 **8. References**

- 18
19 Archer, D., Buffett, B., Brovkin, V. and Schellnhuber, H. J.: Ocean methane hydrates as a
20 slow tipping point in the global carbon cycle, PNAS, 106(49), 20596–20601,
21 doi:10.1073/pnas.0800885105, 2009.
- 22 Aydin, M., Verhulst, K. R., Saltzman, E. S., Battle, M. O., Montzka, S. A., Blake, D. R., Tang, Q.
23 and Prather, M. J.: Recent decreases in fossil-fuel emissions of ethane and methane
24 derived from firn air, Nature, 476(7359), 198–201, doi:10.1038/nature10352, 2011.
- 25 Bièvre, P., Gallet, M., Holden, N. E. and Barnes, I. L.: Isotopic Abundances and Atomic
26 Weights of the Elements, J. Phys. Chem. Ref. Data, 13(3), 809–891,
27 doi:10.1063/1.555720, 1984.
- 28 Bréas, O., Guillou, C., Reniero, F. and Wada, E.: The Global Methane Cycle: Isotopes and
29 Mixing Ratios, Sources and Sinks, Isotopes Environ. Health Stud., 37(4), 257–379,
30 doi:10.1080/10256010108033302, 2001.
- 31 Brown, L. R., Sung, K., Benner, D. C., Devi, V. M., Boudon, V., Gabard, T., Wenger, C.,
32 Campargue, A., Leshchishina, O., Kassi, S., Mondelain, D., Wang, L., Daumont, L., Régalia,
33 L., Rey, M., Thomas, X., Tyuterev, V. G., Lyulin, O. M., Nikitin, A. V, Niederer, H. M., Albert,
34 S., Bauerecker, S., Quack, M., O'Brien, J. J., Gordon, I. E., Rothman, L. S., Sasada, H.,
35 Coustenis, A., Smith, M. A. H., Carrington, T., Wang, X. G., Mantz, A. W. and Spickler, P. T.:
36 Methane line parameters in the HITRAN2012 database, J. Quant. Spectrosc. Radiat.
37 Transf., 130, 201–219, doi:10.1016/j.jqsrt.2013.06.020, 2013.
- 38 Buchwitz, M., Schneising, O., Reuter, M., Heymann, J., Krautwurst, S., Bovensmann, H.,
39 Burrows, J. P., Boesch, H., Parker, R. J., Somkuti, P., Detmers, R. G., Hasekamp, O. P., Aben,
40 I., Butz, A., Frankenberg, C. and Turner, A. J.: Satellite-derived methane hotspot emission
41 estimates using a fast data-driven method, Atmos. Chem. Phys., 17(9), 5751–5774,
42 doi:10.5194/acp-17-5751-2017, 2017.
- 43 Buzan, E. M., Beale, C. A., Boone, C. D. and Bernath, P. F.: Global stratospheric
44 measurements of the isotopologues of methane from the Atmospheric Chemistry
45 Experiment Fourier transform spectrometer, Atmos. Meas. Tech, 9, 1095–1111,
46 doi:10.5194/amt-9-1095-2016, 2016.
- 47 Chanton, J. P.: The effect of gas transport on the isotope signature of methane in
48 wetlands, , doi:10.1016/j.orggeochem.2004.10.007, 2005.

1 Clerbaux, C., Boynard, A., Clarisse, L., George, M., Hadji-Lazaro, J., Herbin, H., Hurtmans,
2 D., Pommier, M., Razavi, A., Turquety, S., Wespes, C. and Coheur, P. F.: Monitoring of
3 atmospheric composition using the thermal infrared IASI/MetOp sounder, *Atmos. Chem.*
4 *Phys.*, 9(16), 6041–6054, doi:10.5194/acp-9-6041-2009, 2009.

5 Craig, H.: Isotopic standards for carbon and oxygen and correction factors for mass-
6 spectrometric analysis of carbon dioxide, *Geochim. Cosmochim. Acta*, 12(1–2), 133–149,
7 doi:10.1016/0016-7037(57)90024-8, 1957.

8 Dudhia, A.: The Reference Forward Model (RFM), *J. Quant. Spectrosc. Radiat. Transf.*,
9 186, 243–253, doi:10.1016/j.jqsrt.2016.06.018, 2017.

10 Etiope, G. and Ciccioli, P.: Earth's Degassing: A Missing Ethane and Propane Source,
11 *Science* (80-.), 323(5913), 478–478, doi:10.1126/science.1165904, 2009.

12 Gordon, I. E., Rothman, L. S., Hill, C., Kochanov, R. V., Tan, Y., Bernath, P. F., Birk, M.,
13 Boudon, V., Campargue, A., Chance, K. V., Drouin, B. J., Flaud, J.-M., Gamache, R. R.,
14 Hodges, J. T., Jacquemart, D., Perevalov, V. I., Perrin, A., Shine, K. P., Smith, M.-A. H.,
15 Tennyson, J., Toon, G. C., Tran, H., Tyuterev, V. G., Barbe, A., Császár, A. G., Devi, V. M.,
16 Furtenbacher, T., Harrison, J. J., Hartmann, J.-M., Jolly, A., Johnson, T. J., Karman, T.,
17 Kleiner, I., Kyuberis, A. A., Loos, J., Lyulin, O. M., Massie, S. T., Mikhailenko, S. N., Moazzen-
18 Ahmadi, N., Müller, H. S. P., Naumenko, O. V., Nikitin, A. V., Polyansky, O. L., Rey, M.,
19 Rotger, M., Sharpe, S. W., Sung, K., Starikova, E., Tashkun, S. A., Auwera, J. Vander,
20 Wagner, G., Wilzewski, J., Wcisło, P., Yu, S. and Zak, E. J.: The HITRAN2016 Molecular
21 Spectroscopic Database, *J. Quant. Spectrosc. Radiat. Transf.*,
22 doi:10.1016/j.jqsrt.2017.06.038, 2017.

23 Herbin, H., Labonnote, L. C. and Dubuisson, P.: Multispectral information from TANSO-
24 FTS instrument – Part 1: Application to greenhouse gases (CO₂ and CH₄) in clear sky
25 conditions, *Atmos. Meas. Tech.*, 6, 3301–3311, doi:10.5194/amt-6-3301-2013, 2013.

26 Holl, G., Walker, K. A., Conway, S., Saitoh, N., Boone, C. D., Strong, K. and Drummond, J. R.:
27 Methane cross-validation between three Fourier transform spectrometers: SCISAT ACE-
28 FTS, GOSAT TANSO-FTS, and ground-based FTS measurements in the Canadian high
29 Arctic, *Atmos. Meas. Tech.*, 9(5), 1961–1980, doi:10.5194/amt-9-1961-2016, 2016.

30 IPCC: Fifth Assessment Report - Impacts, Adaptation and Vulnerability, [online]
31 Available from: <http://www.ipcc.ch/report/ar5/wg2/> (Accessed 12 June 2017), 2014.

32 Irion, F. W., Moyer, E. J., Gunson, M. R., Rinsland, C. P., Yung, Y. L., Michelsen, H. A.,
33 Salawitch, R. J., Chang, A. Y., Newchurch, M. J., Abbas, M. M., Abrams, M. C. and Zander, R.:
34 Stratospheric observations of CH₃D and HDO from ATMOS infrared solar spectra:
35 Enrichments of deuterium in methane and implications for HD, *Geophys. Res. Lett.*,
36 23(17), 2381–2384, doi:10.1029/96GL01402, 1996.

37 Kai, F. M., Tyler, S. C., Randerson, J. T. and Blake, D. R.: Reduced methane growth rate
38 explained by decreased Northern Hemisphere microbial sources, *Nature*, 476(7359),
39 194–197, doi:10.1038/nature10259, 2011.

40 Kneizys, F. X., Anderson, G. P., Shettle, E. P., Gallery, W. O., Abreu, L. W., Selby, J. E. A.,
41 Chetwynd, J. H. and Clough, S. A.: Users guide to LOWTRAN 7., 1988.

42 Kort, E. A., Frankenberg, C., Costigan, K. R., Lindenmaier, R., Dubey, M. K. and Wunch, D.:
43 Four corners: The largest US methane anomaly viewed from space, *Geophys. Res. Lett.*,
44 41(19), 6898–6903, doi:10.1002/2014GL061503, 2014.

45 Kuze, A., Suto, H., Nakajima, M. and Hamazaki, T.: Thermal and near infrared sensor for
46 carbon observation Fourier-transform spectrometer on the Greenhouse Gases
47 Observing Satellite for greenhouse gases monitoring, *Appl. Opt.*, 48(35), 6716,
48 doi:10.1364/AO.48.006716, 2009.

49 Kuze, A., Suto, H., Shiomi, K., Urabe, T., Nakajima, M., Yoshida, J., Kawashima, T.,

1 Yamamoto, Y., Kataoka, F. and Buijs, H.: Level 1 algorithms for TANSO on GOSAT:
2 processing and on-orbit calibrations, *Atmos. Meas. Tech*, 5, 2447–2467,
3 doi:10.5194/amt-5-2447-2012, 2012.

4 De Lange, A. and Landgraf, J.: Methane profiles from GOSAT thermal infrared spectra,
5 *Atmos. Meas. Tech.*, 11(6), 3815–3828, doi:10.5194/amt-11-3815-2018, 2018.

6 Leifer, I., Roberts, D., Margolis, J. and Kinnaman, F.: In situ sensing of methane emissions
7 from natural marine hydrocarbon seeps: A potential remote sensing technology, *Earth*
8 *Planet. Sci. Lett.*, 245(3–4), 509–522, doi:10.1016/j.epsl.2006.01.047, 2006.

9 Malina, E., Yoshida, Y., Matsunaga, T. and Muller, J. P.: Information content analysis: The
10 potential for methane isotopologue retrieval from GOSAT-2, *Atmos. Meas. Tech.*, 11(2),
11 1159–1179, doi:10.5194/amt-11-1159-2018, 2018.

12 McNorton, J., Chipperfield, M. P., Gloor, M., Wilson, C., Feng, W., Hayman, G. D., Rigby, M.,
13 Krummel, P. B., O’Doherty, S., Prinn, R. G., Weiss, R. F., Young, D., Dlugokencky, E. and
14 Montzka, S. A.: Role of OH variability in the stalling of the global atmospheric CH₄
15 growth rate from 1999 to 2006, *Atmos. Chem. Phys*, 16, 7943–7956, doi:10.5194/acp-
16 16-7943-2016, 2016.

17 Muller, J.-P., Lewis, P., Bréon, F.-M., Bacour, C., Price, I., Chaumat, L., Prunet, P., Gonzales,
18 L., Schlundt, C., Vountas, M., Burrows, J., von Hoyningen-Huene, W., Guanter, L., Fischer,
19 J., North, P., Heckel, A. and Straume-Lindner, A. G.: A Surface Reflectance Database for
20 ESA’s Earth Observation Missions (ADAM), ESA Living Planet Symposium, Edinburgh,
21 2013.

22 Nisbet, E. G., Dlugokencky, E. J., Manning, M. R., Lowry, D., Fisher, R. E., France, J. L.,
23 Michel, S. E., Miller, J. B., White, J. W. C., Vaughn, B., Bousquet, P., Pyle, J. A., Warwick, N. J.,
24 Cain, M., Brownlow, R., Zazzeri, G., Lanoisellé, M., Manning, A. C., Gloor, E., Worthy, D. E. J.,
25 Brunke, E.-G., Labuschagne, C., Wolff, E. W. and Ganesan, A. L.: Rising atmospheric
26 methane: 2007-2014 growth and isotopic shift, *Global Biogeochem. Cycles*, 30(9), 1356–
27 1370, doi:10.1002/2016GB005406, 2016.

28 Ohyama, H., Kawakami, S., Shiomi, K., Morino, I. and Uchino, O.: Atmospheric
29 Temperature and Water Vapor Retrievals from GOSAT Thermal Infrared Spectra and
30 Initial Validation with Coincident Radiosonde Measurements, *SOLA*, 9(0), 143–147,
31 doi:10.2151/sola.2013-032, 2013.

32 Ohyama, H., Kawakami, S., Shiomi, K., Morino, I. and Uchino, O.: Intercomparison of XH₂O
33 data from the GOSAT TANSO-FTS (TIR and SWIR) and ground-based FTS measurements:
34 Impact of the spatial variability of XH₂O on the intercomparison, *Remote Sens.*, 9(1), 64,
35 doi:10.3390/rs9010064, 2017.

36 Parker, R., Boesch, H., Cogan, A., Fraser, A., Feng, L., Palmer, P. I., Messerschmidt, J.,
37 Deutscher, N., Griffith, D. W. T., Notholt, J., Wennberg, P. O. and Wunch, D.: Methane
38 observations from the Greenhouse Gases Observing SATellite: Comparison to ground-
39 based TCCON data and model calculations, *Geophys. Res. Lett.*, 38(15),
40 doi:10.1029/2011GL047871, 2011.

41 Parker, R. J., Boesch, H., Byckling, K., Webb, A. J., Palmer, P. I., Feng, L., Bergamaschi, P.,
42 Chevallier, F., Notholt, J., Deutscher, N., Warneke, T., Hase, F., Sussmann, R., Kawakami, S.,
43 Kivi, R., Griffith, D. W. T. and Velasco, V.: Assessing 5 years of GOSAT Proxy XCH₄ data
44 and associated uncertainties, *Atmos. Meas. Tech*, 8, 4785–4801, doi:10.5194/amt-8-
45 4785-2015, 2015.

46 Parker, R. J., Boesch, H., Wooster, M. J., Moore, D. P., Webb, A. J., Gaveau, D., Murdiyarso,
47 D. and Parker, R.: Atmospheric CH₄ and CO₂ enhancements and biomass burning
48 emission ratios derived from satellite observations of the 2015 Indonesian fire plumes,
49 *Atmos. Chem. Phys*, 16, 10111–10131, doi:10.5194/acp-16-10111-2016, 2016.

1 Rella, C. W., Crosson, E., Jacobson, G., Karion, A., Petron, G. and Sweeney, C.: Quantifying
2 the relative contribution of natural gas fugitive emissions to total methane emissions in
3 Colorado and Utah using mobile d 13 CH 4 analysis, pp. 12–1, EGU, Vienna, 2013.

4 Remedios, J. J., Leigh, R. J., Waterfall, A. M., Moore, D. P., Sembhi, H., Parkes, I.,
5 Greenhough, J., Chipperfield, M. P. and Hauglustaine, D.: MIPAS reference atmospheres
6 and comparisons to V4.61/V4.62 MIPAS level 2 geophysical data sets, *Atmos. Chem.*
7 *Phys. Discuss. Eur. Geosci. Union*, 7(4), 9973–10017, doi:10.5194/acpd-7-9973-2007,
8 2007.

9 Reuter, M., Bovensmann, H., Buchwitz, M., Burrows, J. P., Deutscher, N. M., Heymann, J.,
10 Rozanov, A., Schneising, O., Suto, H., Toon, G. C. and Warneke, T.: On the potential of the
11 2041-2047nm spectral region for remote sensing of atmospheric CO 2 isotopologues, *J.*
12 *Quant. Spectrosc. Radiat. Transf.*, 113(16), 2009–2017, doi:10.1016/j.jqsrt.2012.07.013,
13 2012.

14 Rigby, M., Manning, A. J. and Prinn, R. G.: The value of high-frequency, high-precision
15 methane isotopologue measurements for source and sink estimation, *J. Geophys. Res.*
16 *Atmos.*, 117(12), doi:10.1029/2011JD017384, 2012.

17 Roberts, D. A., Bradley, E. S., Cheung, R., Leifer, I., Dennison, P. E. and Margolis, J. S.:
18 Mapping methane emissions from a marine geological seep source using imaging
19 spectrometry, *Remote Sens. Environ.*, 114(3), 592–606, doi:10.1016/j.rse.2009.10.015,
20 2010.

21 Röckmann, T., Brass, M., Borchers, R. and Engel, A.: The isotopic composition of methane
22 in the stratosphere: High-altitude balloon sample measurements, *Atmos. Chem. Phys.*,
23 11(24), 13287–13304, doi:10.5194/acp-11-13287-2011, 2011.

24 Rodgers, C. D.: *Inverse Methods for Atmospheric Sounding - Theory and Practice*, World
25 Scientific., 2000.

26 Rothman, L. S., Gordon, I. E., Barbe, A., Benner, D. C., Bernath, P. F., Birk, M., Boudon, V.,
27 Brown, L. R., Campargue, A., Champion, J.-P., Chance, K., Coudert, L. H., Dana, V., Devi, V.
28 M., Fally, S., Flaud, J.-M., Gamache, R. R., Goldman, A., Jacquemart, D., Kleiner, I., Lacome,
29 N., Lafferty, W. J., Mandin, J.-Y., Massie, S. T., Mikhailenko, S. N., Miller, C. E., Moazzen-
30 Ahmadi, N., Naumenko, O. V., Nikitin, A. V., Orphal, J., Perevalov, V. I., Perrin, A., Predoi-
31 Cross, A., Rinsland, C. P., Rotger, M., Šimečková, M., Smith, M. A. H., Sung, K., Tashkun, S.
32 A., Tennyson, J., Toth, R. A., Vandaele, A. C. and Vander Auwera, J.: The HITRAN 2008
33 molecular spectroscopic database, *J. Quant. Spectrosc. Radiat. Transf.*, 110(9–10), 533–
34 572, doi:10.1016/j.jqsrt.2009.02.013, 2009.

35 Rozanov, V. V., Rozanov, A. V., Kokhanovsky, A. A. and Burrows, J. P.: Radiative transfer
36 through terrestrial atmosphere and ocean: Software package SCIATRAN, *J. Quant.*
37 *Spectrosc. Radiat. Transf.*, 133, 13–71, doi:10.1016/j.jqsrt.2013.07.004, 2014.

38 Schepers, D., Guerlet, S., Butz, A., Landgraf, J., Frankenberg, C., Hasekamp, O., Blavier, J. F.,
39 Deutscher, N. M., Griffith, D. W. T., Hase, F., Kyro, E., Morino, I., Sherlock, V., Sussmann, R.
40 and Aben, I.: Methane retrievals from Greenhouse Gases Observing Satellite (GOSAT)
41 shortwave infrared measurements: Performance comparison of proxy and physics
42 retrieval algorithms, *J. Geophys. Res. Atmos.*, 117(10), doi:10.1029/2012JD017549,
43 2012.

44 Schweizer, M., Fear, J. and Cadisch, G.: Isotopic (13C) fractionation during plant residue
45 decomposition and its implications for soil organic matter studies, *Rapid Commun. Mass*
46 *Spectrom.*, 13(13), 1284–1290, doi:10.1002/(SICI)1097-
47 0231(19990715)13:13<1284::AID-RCM578>3.0.CO;2-0, 1999.

48 Schwietzke, S., Sherwood, O. A., Bruhwiler, L. M. P., Miller, J. B., Etiope, G., Dlugokencky, E.
49 J., Michel, S. E., Arling, V. A., Vaughn, B. H., White, J. W. C. and Tans, P. P.: Upward revision

1 of global fossil fuel methane emissions based on isotope database, *Nature*, 538(7623),
2 88–91, doi:10.1038/nature19797, 2016.

3 Sinnhuber, B. M., Sheode, N., Sinnhuber, M., Chipperfield, M. P. and Feng, W.: The
4 contribution of anthropogenic bromine emissions to past stratospheric ozone trends: A
5 modelling study, *Atmos. Chem. Phys.*, 9(8), 2863–2871, doi:10.5194/acp-9-2863-2009,
6 2009.

7 Starikova, E., Nikitin, A. V., Rey, M., Tashkun, S. A., Mondelain, D., Kassi, S., Campargue, A.
8 and Tyuterev, V. G.: Assignment and modeling of the absorption spectrum of $^{13}\text{CH}_4$ at 80
9 K in the region of the $2\nu_3$ band (5853–6201 cm^{-1}), *J. Quant. Spectrosc. Radiat. Transf.*,
10 177, 170–180, doi:10.1016/j.jqsrt.2015.12.023, 2016.

11 Turner, A. J., Jacob, D. J., Wecht, K. J., Maasakkers, J. D., Lundgren, E., Andrews, A. E.,
12 Biraud, S. C., Boesch, H., Bowman, K. W., Deutscher, N. M., Dubey, M. K., Griffith, D. W. T.,
13 Hase, F., Kuze, A., Notholt, J., Ohyama, H., Parker, R., Payne, V. H., Sussmann, R., Sweeney,
14 C., Velasco, V. A., Warneke, T., Wennberg, P. O. and Wunch, D.: Estimating global and
15 North American methane emissions with high spatial resolution using GOSAT satellite
16 data, *Atmos. Chem. Phys.*, 15(12), 7049–7069, doi:10.5194/acp-15-7049-2015, 2015.

17 Turner, A. J., Frankenberg, C., Wennberg, P. O. and Jacob, D. J.: Ambiguity in the causes for
18 decadal trends in atmospheric methane and hydroxyl., *Proc. Natl. Acad. Sci. U. S. A.*,
19 114(21), 5367–5372, doi:10.1073/pnas.1616020114, 2017.

20 Weidmann, D., Hoffmann, A., Macleod, N., Middleton, K., Kurtz, J., Barraclough, S. and
21 Griffin, D.: The Methane Isotopologues by Solar Occultation (MISO) Nanosatellite
22 Mission: Spectral Channel Optimization and Early Performance Analysis, *Remote Sens.*,
23 9(10), 1073, doi:10.3390/rs9101073, 2017.

24 Whiticar, M. J.: Carbon and hydrogen isotope systematics of bacterial formation and
25 oxidation of methane, *Chem. Geol.*, 161(1–3), 291–314, doi:10.1016/S0009-
26 2541(99)00092-3, 1999.

27 Worden, J. R., Turner, A. J., Bloom, A., Kulawik, S. S., Liu, J., Lee, M., Weidner, R., Bowman,
28 K., Frankenberg, C., Parker, R. and Payne, V. H.: Quantifying lower tropospheric methane
29 concentrations using GOSAT near-IR and TES thermal IR measurements, *Atmos. Meas.*
30 *Tech*, 8, 3433–3445, doi:10.5194/amt-8-3433-2015, 2015.

31 Wuebbles, D. and Hayhoe, K.: Atmospheric methane and global change, *Earth-Science*
32 *Rev.*, 57(3–4), 177–210, doi:10.1016/S0012-8252(01)00062-9, 2002.

33 Wunch, D., Toon, G. C., Blavier, J.-F. L., Washenfelder, R. A., Notholt, J., Connor, B. J.,
34 Griffith, D. W. T., Sherlock, V. and Wennberg, P. O.: The Total Carbon Column Observing
35 Network, *Phil. Trans. R. Soc. A*, 369, 2087–2112, doi:10.1098/rsta.2010.0240, 2011.

36 Yokota, T., Yoshida, Y., Eguchi, N., Ota, Y., Tanaka, T., Watanabe, H. and Maksyutov, S.:
37 Global Concentrations of CO_2 and CH_4 Retrieved from GOSAT: First Preliminary Results,
38 *SOLA*, 5, 160–163, doi:10.2151/sola.2009-041, 2009.

39 Yoshida, Y., Ota, Y., Eguchi, N., Kikuchi, N., Nobuta, K., Tran, H., Morino, I. and Yokota, T.:
40 Retrieval algorithm for CO_2 and CH_4 column abundances from short-wavelength
41 infrared spectral observations by the Greenhouse gases observing satellite, *Atmos. Meas.*
42 *Tech*, 4, 717–734, doi:10.5194/amt-4-717-2011, 2011.

43 Yoshida, Y., Kikuchi, N., Morino, I., Uchino, O., Oshchepkov, S., Bril, A., Saeki, T., Schutgens,
44 N., Toon, G. C., Wunch, D., Roehl, C. M., Wennberg, P. O., Griffith, D. W. T., Deutscher, N. M.,
45 Warneke, T., Notholt, J., Robinson, J., Sherlock, V., Connor, B., Rettinger, M., Sussmann, R.,
46 Ahonen, P., Heikkinen, P., Kyrö, E., Mendonca, J., Strong, K., Hase, F., Dohe, S. and Yokota,
47 T.: Improvement of the retrieval algorithm for GOSAT SWIR XCO_2 and XCH_4 and their
48 validation using TCCON data, *Atmos. Meas. Tech.*, 6(6), 1533–1547, doi:10.5194/amt-6-
49 1533-2013, 2013.

1 Zou, M., Xiong, X., Saitoh, N., Warner, J., Zhang, Y., Chen, L., Weng, F. and Fan, M.: Satellite
2 observation of atmospheric methane: intercomparison between AIRS and GOSAT
3 TANSO-FTS retrievals, *Atmos. Meas. Tech.*, 9, 3567–3576, doi:10.5194/amt-9-3567-
4 2016, 2016.

5
6
7
8
9
10
11
12
13
14
15
16
17
18
19
20
21
22
23
24
25
26
27
28
29
30
31
32
33
34
35
36
37
38
39
40
41
42
43
44
45
46
47
48
49

1 **Tables**

2
3 **Table 1. The conditions used by ORFM in generating SWIR Absorption from an assumed GOSAT-TANSO-FTS like**
4 **instrument. All conditions are taken from MIPAS Model atmospheres (46).**

5

Condition Variables	Value
Wavelength Range	1600-1700 nm 7600 – 8300 nm
Background Gases	H ₂ O, CO ₂ and N ₂ O at standard model concentrations
Instrument Altitude	666km
Solar Zenith Angle	30°
Atmospheric Model	University of Leicester MIPAS Model
Spectral Line Database	HITRAN 2016
Spectral Resolution	0.01cm ⁻¹
Viewing Profile	Nadir

6
7 **Table 2. SCIATRAN Simulation conditions for detection study.**

Sensor	Surface/Atmosphere	Notes
Solar Zenith: 30° Altitude: 666 km	Background Conditions	
	Reflectance: 0.1, 0.3 - 0.6	
	H ₂ O: As SCIATRAN CTM (November, Latitude 45°)	
	CH ₄ : As SCIATRAN CTM (November, Latitude 45°)	
	Aerosols: As LOWTRAN SCIATRAN standard settings	Maritime/tropospheric in the boundary layer. Background in the stratosphere.
	Elevated Conditions	
	Reflectance: 0.1, 0.3, 0.6	Vegetation to Desert.
	H ₂ O: As background x2	Not necessarily realistic, but indicates sensitivity to water vapour.
	CH ₄ Scale Factor: 1.02, 1.04, 1.06, 1.08, 1.10	XCH ₄ values, minimum 1.78 ppm, maximum 1.94 ppm.

8
9
10 **Table 3. Spectral average F_d (Equation 4) values summarised for the standard conditions expressed Table 2. The F_d**
11 **values are shown for each CH₄ scale given the range of reflectances indicated in Table 1.**

CH ₄ Total Column Scale Factor	F _d Albedo = 0.1 (x10 ⁻¹⁰)	F _d Albedo = 0.3 (x10 ⁻¹⁰)	F _d Albedo = 0.4 (x10 ⁻¹⁰)	F _d Albedo = 0.5 (x10 ⁻¹⁰)	F _d Albedo = 0.6 (x10 ⁻¹⁰)
1658.6 – 1658.65 nm					
x1.02	-1.41	-1.19	-1.08	-0.975	-0.864
x1.04	-1.30	-0.87	-0.652	-0.432	-0.211
x1.06	-1.19	-0.546	-0.219	0.110	0.444
x1.08	-1.08	-0.223	0.213	0.652	1.10
x1.10	-0.974	0.0999	0.644	1.19	1.75
1670.35 – 1670.55 nm					
x1.02	-1.42	-1.23	-1.13	-1.03	-0.931
x1.04	-1.32	-0.938	-0.742	-0.545	-0.346

x1.06	-1.23	-0.648	-0.355	-0.0582	0.241
x1.08	-1.13	-0.358	0.0327	0.428	0.827
x1.10	-1.03	-0.0688	0.420	0.913	1.41

1
2
3
4
5
6
7
8
9
10

Table 4. Spectral average F_d (Equation 4) values summarised for the standard conditions expressed Table 2, assuming a global standard $\delta^{13}C$ value of -70. The F_d values are shown for each CH_4 scale given the range of reflectances indicated in Table 2.

CH₄ Total Column Scale Factor	F_d Albedo = 0.1 (x10⁻¹⁰)	F_d Albedo = 0.3 (x10⁻¹⁰)	F_d Albedo = 0.4 (x10⁻¹⁰)	F_d Albedo = 0.5 (x10⁻¹⁰)	F_d Albedo = 0.6 (x10⁻¹⁰)
1658.6 – 1658.65 nm					
x1.02	-1.51	-1.49	-1.47	-1.46	-1.45
x1.04	-1.50	-1.45	-1.43	-1.41	-1.39
x1.06	-1.48	-1.42	-1.39	-1.35	-1.32
x1.08	-1.47	-1.39	-1/34	-1.30	-1.25
x1.10	-1.46	-1.36	-1.30	-1.25	-1.19
1670.35 – 1670.55 nm					
x1.02	-1.42	-1.22	-1.12	-1.03	-0.924
x1.04	-1.32	-0.93	-0.733	-0.535	-0.330
x1.06	-1.22	-0.636	-0.341	-0.043	0.263
x1.08	-1.12	-0.343	0.0512	0.448	0.857
x1.10	-1.02	-0.0494	0.443	0.939	1.450

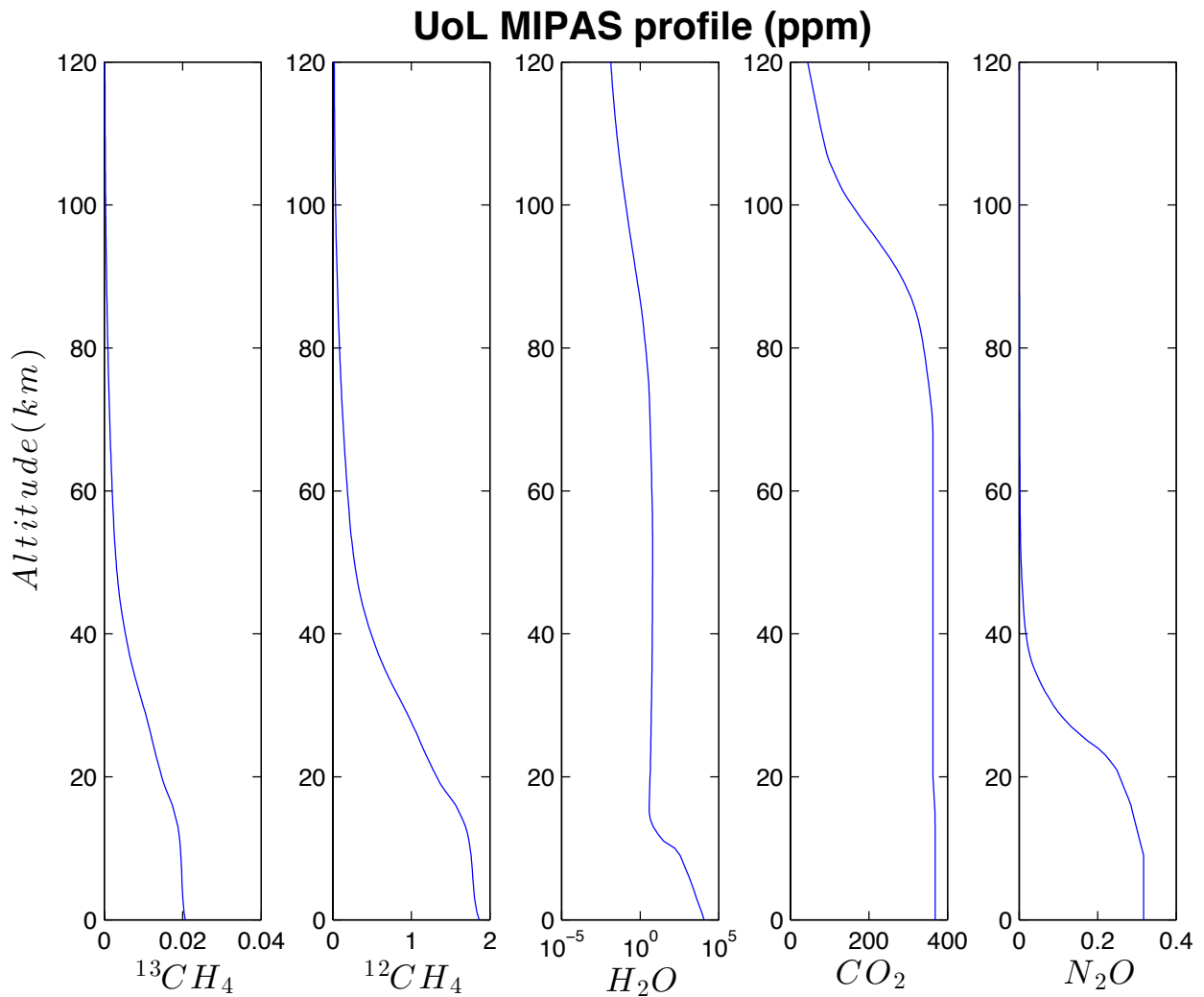
11
12
13
14
15
16
17
18
19
20

Table 5. Sensitivity factor for the 1658 nm and 1670 nm wavebands, assuming the low and high water vapour conditions, and a surface albedo of 0.3 specified in Table 2.

Waveband/Methane scale	Scale = 2%	Scale = 4%	Scale = 6%	Scale = 8%	Scale = 10%
1658.6 nm S_f	1.00121	1.00126	1.00127	1.00125	1.00125
1670.35 nm S_f	1.0113	1.00113	1.0113	1.0112	1.0112

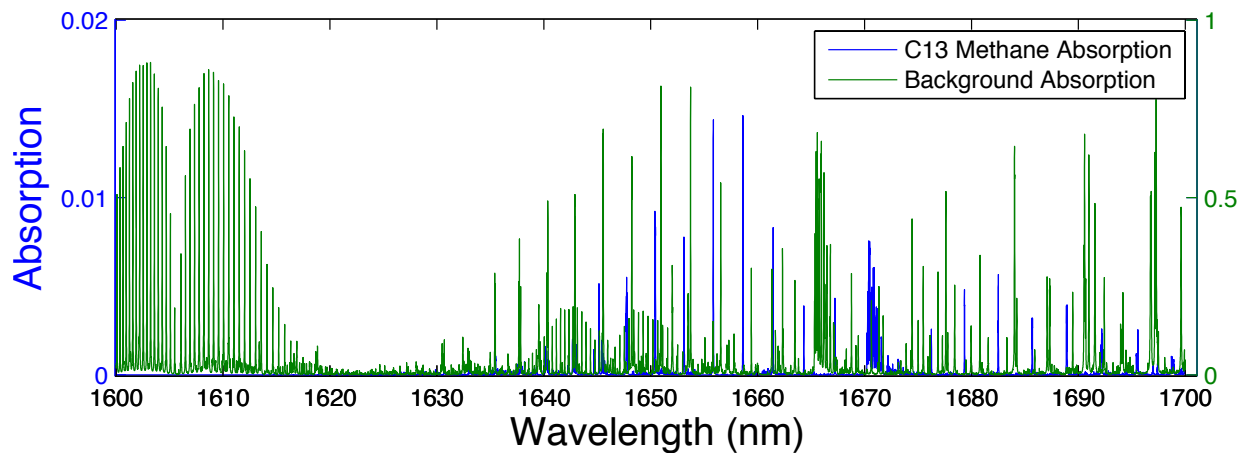
21
22
23
24
25
26

1
2
Figures



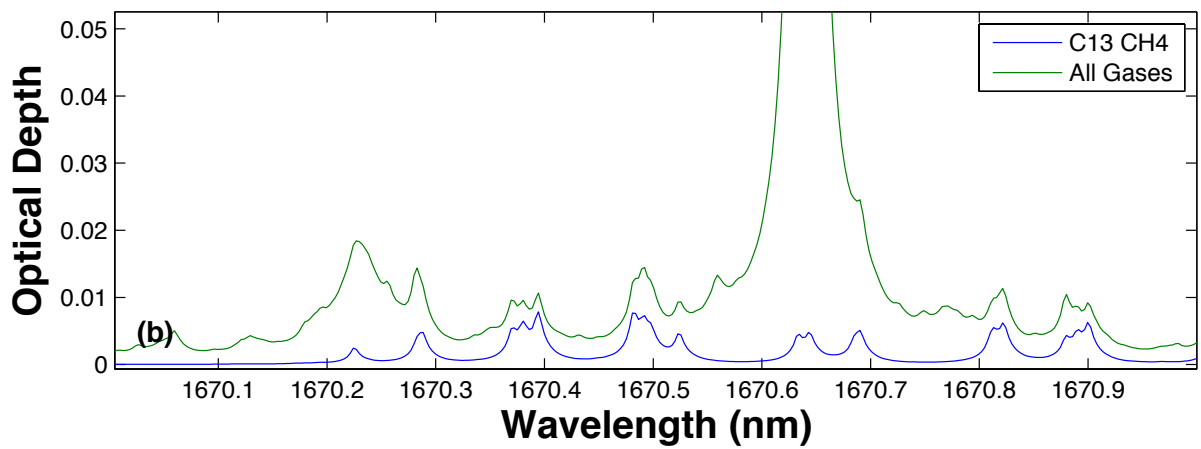
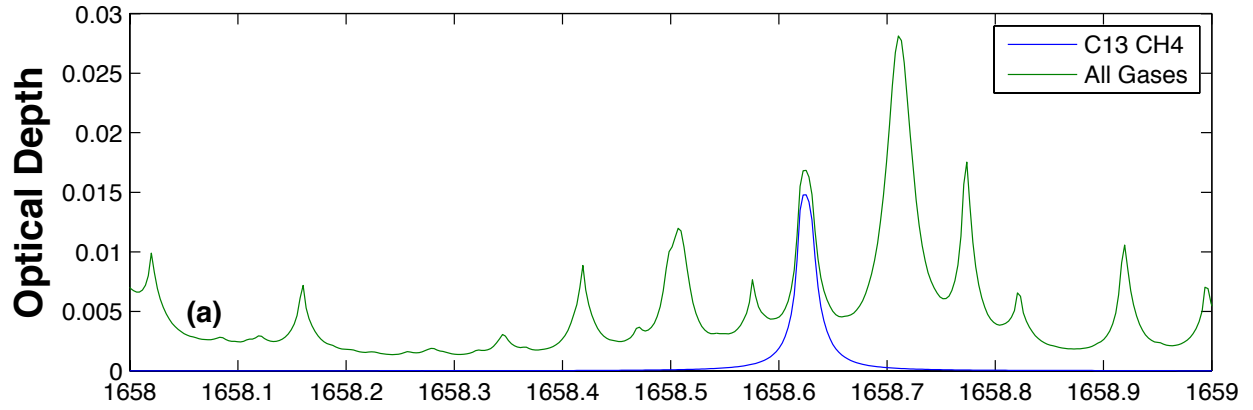
3
4
5

Figure 1. Volume Mixing Ratio profiles of the main gases of interest CH_4 , H_2O and CO_2 in ppm from 0-120km altitude, (46), adapted from (21).

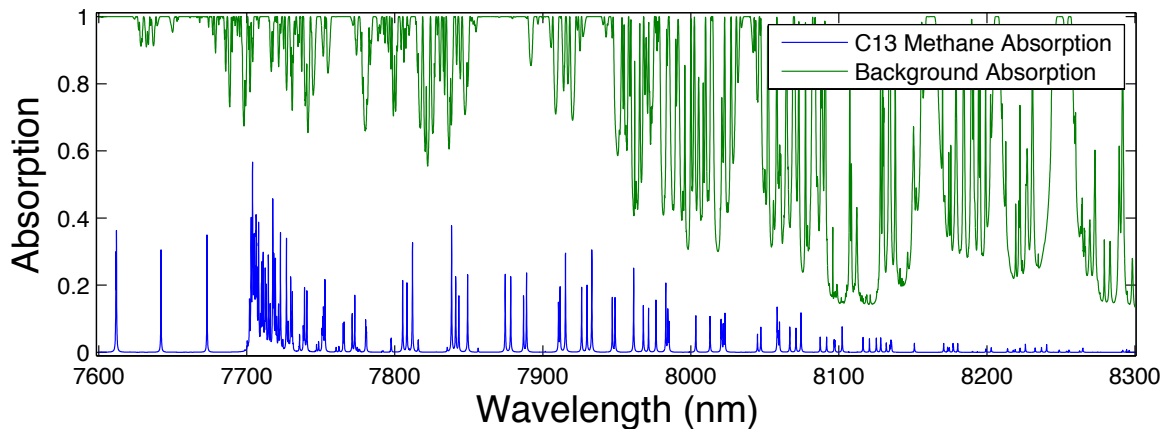


6
7
8
9
10

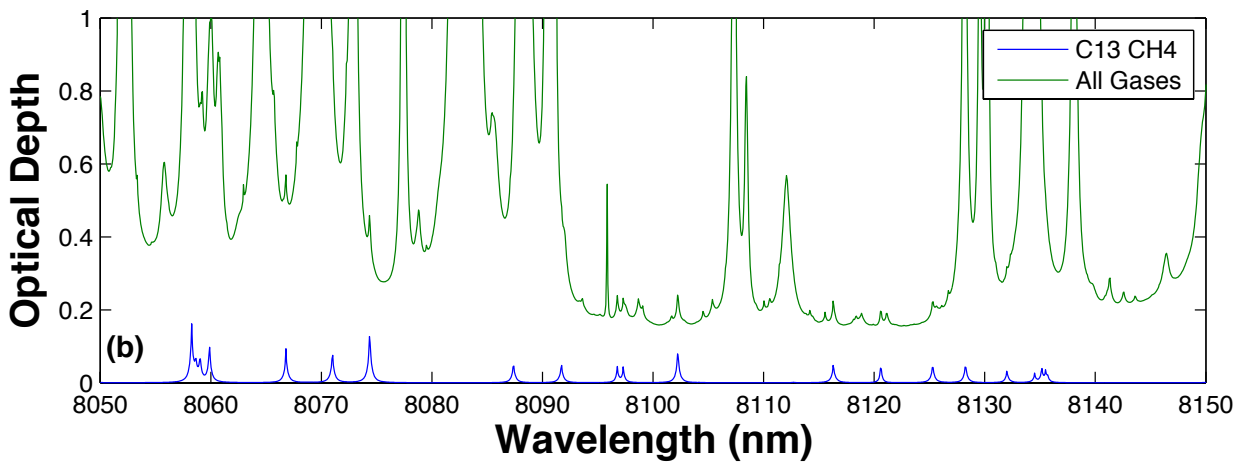
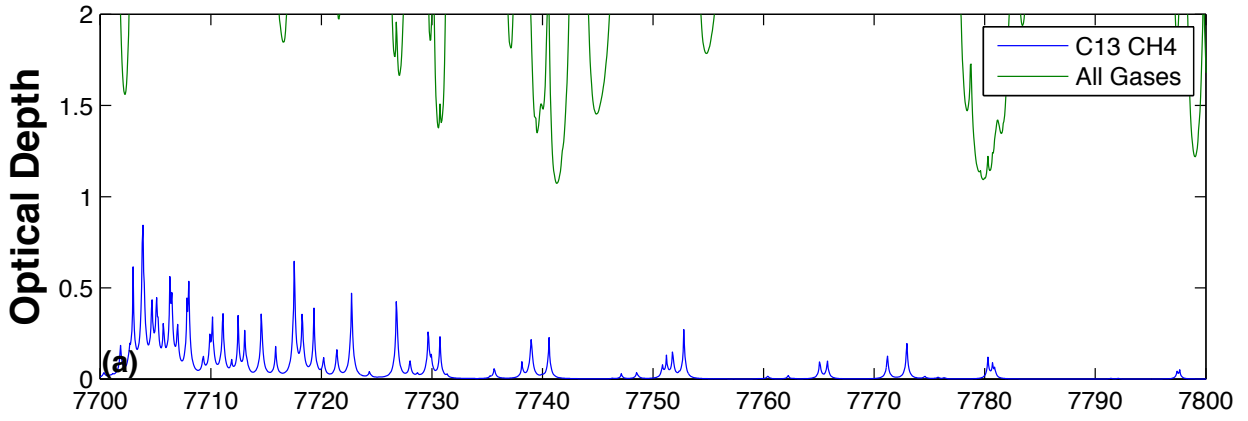
Figure 2. Simulated absorption spectrum from ORFM in the wavelength range 1600-1700nm, the y scale represents the fraction of radiation absorbed by the molecules under investigation. The blue line represents absorption by $^{13}\text{CH}_4$ (left hand scale) and green represents all other key absorbing background gases (CO_2 , H_2O and $^{12}\text{CH}_4$) (right hand scale).



1
2
3
4
5
6
Figure 3. Optical depth covering $^{13}\text{CH}_4$ absorption points of interest, the green line represents optical depth of all gases present in this portion of the spectrum (CH_4 , CO_2 and H_2O), whilst the blue line shows optical depth of purely the methane isotopologue $^{13}\text{CH}_4$: (a) indicates optical depth in the wavelength range 1658-1659nm; (b) shows optical depth in the wavelength range 1670-1671nm. This figure is as figure 5 in (21), but has been updated to reflect the use of HITRAN2016.

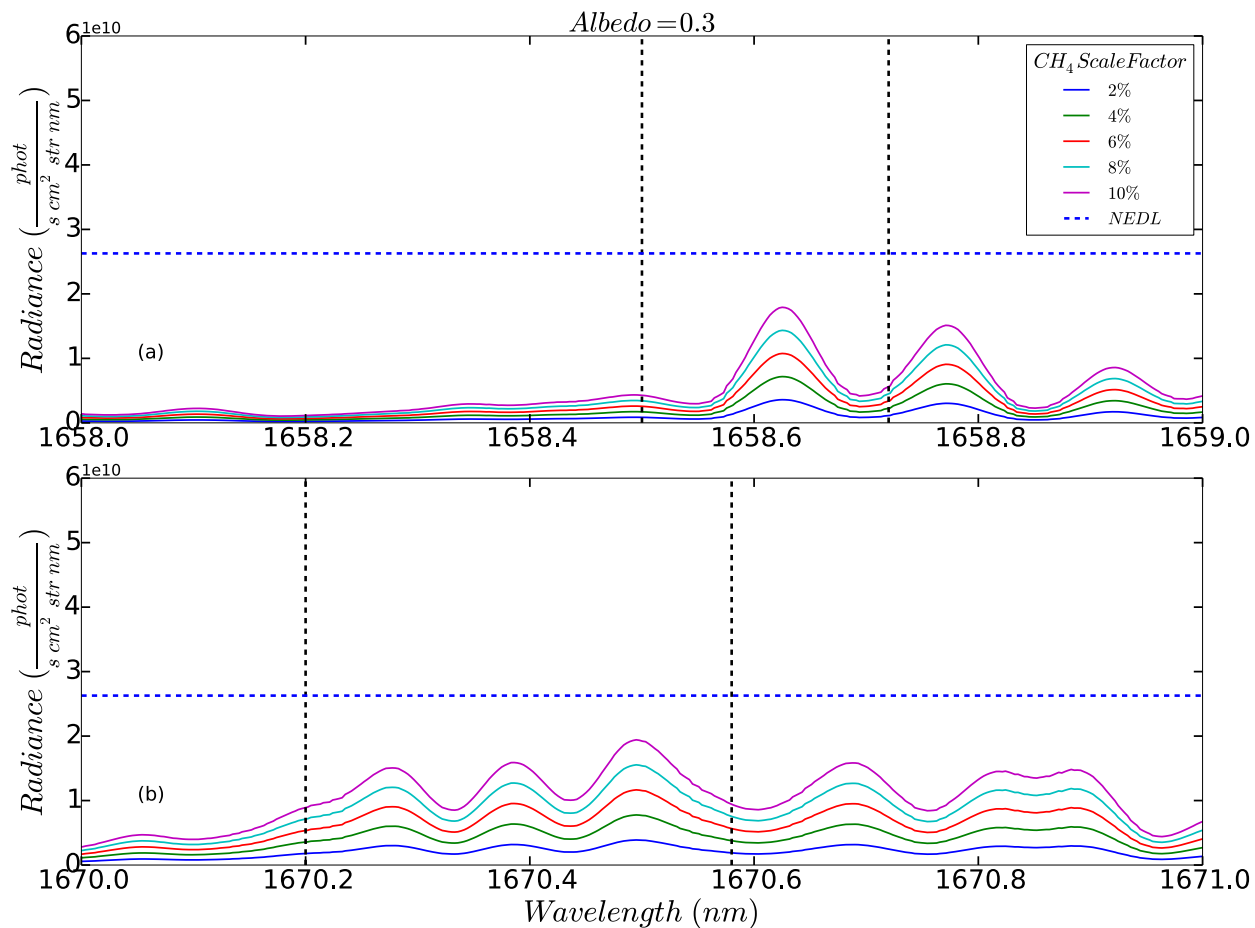


7
8
9
10
Figure 4. Simulated absorption spectrum from ORFM in the wavelength range 7600-8300 nm, the y scale represents the fraction of radiation absorbed by the molecules under investigation. The blue line represents absorption by $^{13}\text{CH}_4$ and green represents all other key absorbing background gases (CO_2 , H_2O , N_2O and $^{12}\text{CH}_4$).



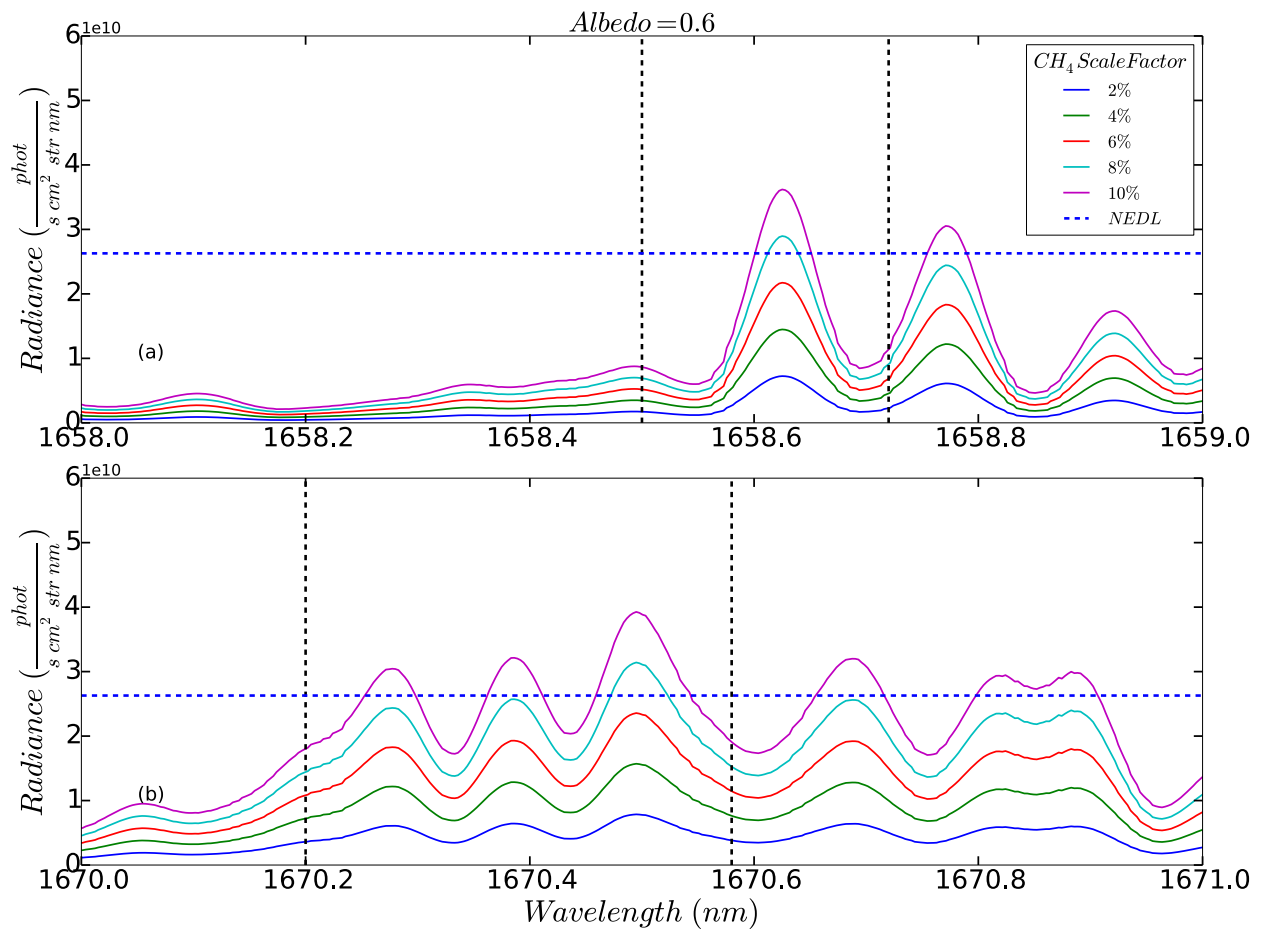
1
2
3

Figure 5. As figure 3, but focused on the wavelength ranges 7700-7800 nm and 8050-8150 nm.



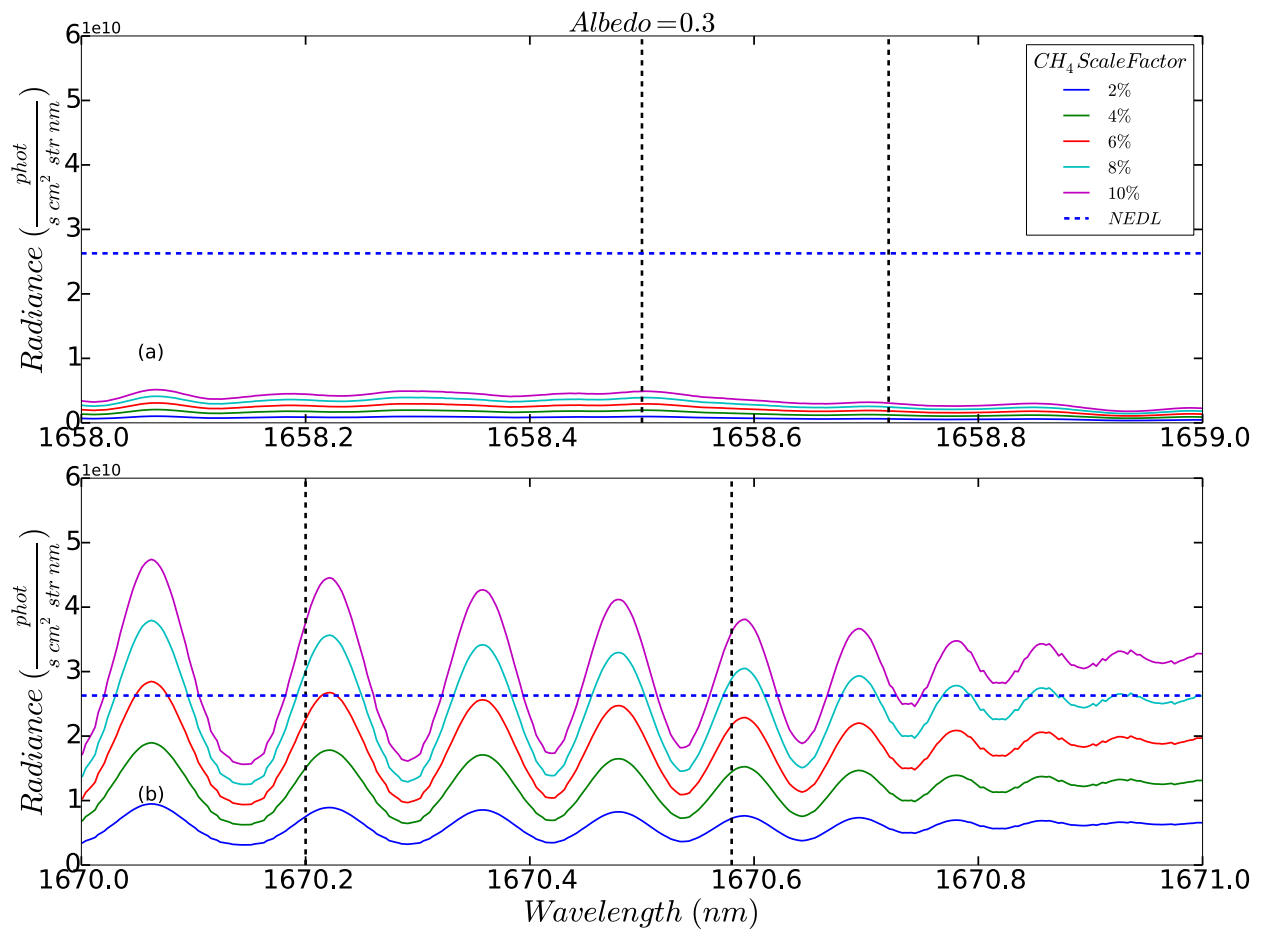
1
2
3
4
5
6
7

Figure 6. Residual Radiance plots based on the simulation conditions highlighted in Table 3, where simulated radiance from the background conditions under the standard ‘day’ scene with a reflectance of 0.3 are subtracted from elevated methane conditions. The residual radiance values are represented by the lines indicated in the legend. The Blue dashed line represents the NEDL. The solid vertical dashed lines identify the regions where $^{13}\text{CH}_4$ spectral lines are prevalent: (a) highlights the $^{13}\text{CH}_4$ spectral line in the 1658-1659 nm range; (b) focuses on the $^{13}\text{CH}_4$ spectral line in the 1670-1671 nm range.



1

2 Figure 7. As Figure 6, with surface albedo increased to 0.6.



1
2
3

Figure 8. As Figure 6 and Figure 7, with surface albedo increased to 0.3, assuming the standard $\delta^{13}\text{C}$ value is -70‰ as opposed to 0‰.

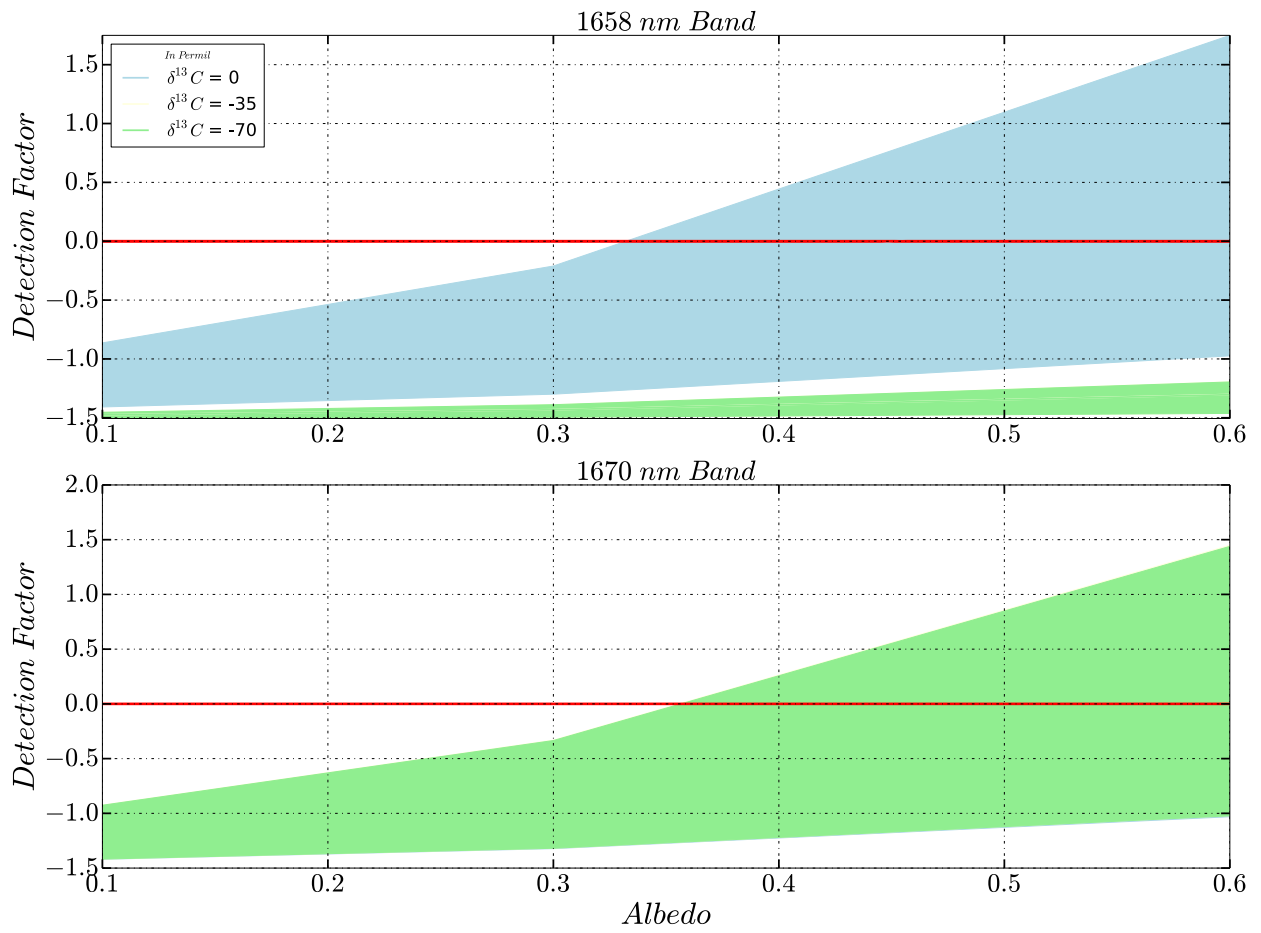


Figure 9. Plot indicating the surface conditions required to generate detection factors > 0 , thus suggesting a positive detection of $\delta^{13}\text{C}$. The top panel shows results for the 1658 nm band, and the bottom panel shows results for the 1670 nm band. The light blue area indicates results assuming a $\delta^{13}\text{C}$ natural value of 0‰, light yellow -35‰ and light green -70‰, the solid red line indicates where the detection factor is zero.

1
2
3
4
5
6
7
8
9
10
11
12
13
14
15
16